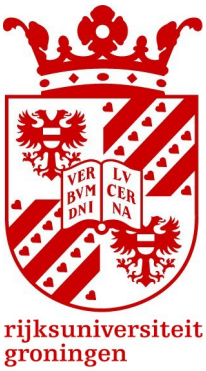

UNIVERSITY OF GRONINGEN

MASTER THESIS

High Accuracy Calculations for the Selection of Promising Candidates for Measurement of NSD-PV Effects in Molecules

Author:
Pablo CAPARRÓS CALLE *(S3695778)*

First Examiner:
prof. dr. ANASTASIA BORSCHEVSKY

Second Examiner:
prof. dr. STEVEN HOEKSTRA

Daily Supervisor:
prof dr. LUKÁŠ FÉLIX PAŠTEKA

Date:
July 2024

High Accuracy Calculations for the Selection of Promising Candidates for Measurement of NSD-PV Effects in Molecules

Quantifying the NSD-PV Enhancement Factor (W_{PV}) of Fluorine and Its Impact on Diatomic Molecules

Pablo Caparrós Calle

Abstract

This study investigates the enhancement factor W_{PV} of the fluorine atom across various diatomic molecular systems using diverse computational methods, including DHF, MP2, CCSD, and CCSD(T). Calculations were performed using the DIRAC quantum chemistry program and the relativistic Dyall basis set. For SrF, the enhancement factors for both nuclei were calculated, resulting in W_{PV} values of 0.240 ± 0.028 Hz for F and 63.1 ± 5.2 Hz for Sr, indicating a significantly higher sensitivity of the metal atom to NSD-PV effects. Computational parameters were adjusted, focusing on electron correlation treatment, active space size, and basis set quality. The results emphasize the substantial impact of electron correlation treatment on W_{PV}, with fluorine's response being notably influenced by core electron correlations and the computational method used. The inclusion of triple excitations further altered the values, particularly affecting the fluorine atom and underscoring it as a primary source of uncertainty. Comparative studies of different molecular isoelectronic pairs (SrF, YF+, CF, and NF+) and XeF further illustrate the distinct behavior of W_{PV} in the fluorine atom across different molecular environments. These findings underscore the importance of precise computational methodologies in elucidating atomic interactions and provide valuable insights for future research in computational chemistry and atomic physics. This comprehensive analysis not only highlights the necessity of accurate electron correlation treatment but also demonstrates the varying sensitivities of enhancement factors depending on the molecular context.

Contents

1 Introduction **3**

2 Theory **6**
2.1 PV Hamiltonian . . . 6
2.2 Nuclear Spin Dependent Effects . . . 7
2.2.1 Nuclear Anapole Moment . . . 7
2.3 First-order Perturbation on Model Hamiltonian . . . 8
2.3.1 Finite Field Method . . . 8

3 Computational Methods and Considerations **10**
3.1 Born-Oppenheimer Approximation . . . 10
3.1.1 One-Electron Operator . . . 11
3.1.2 Two-Electron Operator . . . 12
3.2 Molecular Orbital Theory . . . 12
3.2.1 Basis Sets . . . 12
3.2.2 Dyall Basis Sets . . . 14
3.3 Computational Methods . . . 15
3.3.1 Hartree-Fock . . . 15
3.3.2 Restricted and Unrestricted Hartree-Fock . . . 17
3.3.3 Dirac-Hartree-Fock . . . 17
3.3.4 Electron Correlation Methods . . . 17
3.3.5 Coupled Cluster . . . 17
3.3.6 Møller-Plesset Perturbation Theory . . . 18

4 Results **20**
4.1 Molecular Geometries . . . 20
4.2 Calculations for the Enhancement Factor W_{PV} in SrF . . . 20
4.2.1 Basis Set Quality . . . 21
4.2.2 Electron Correlation and Virtual Space Cut-off . . . 23
4.2.3 Computational Method . . . 26
4.3 Calculation of the Enhancement Factor W_{PV} for Fluorine in Various Molecular Systems . . . 28

5 Discussion **29**
5.1 SrF and Computational Parameters . . . 29
5.2 Uncertainty . . . 30
5.3 Other Molecular Systems . . . 31

6 Conclusion **33**

7 References **34**

1 Introduction

The Standard Model (SM) of particle physics is the cornerstone of modern theoretical physics. It elegantly encapsulates the fundamental constituents of matter and their interactions within the framework of quantum field theory. Nevertheless, despite its remarkable predictive power, the SM encounters some limitations. The most notable ones are its inability to reconcile gravity with the other fundamental forces, its inability to account for phenomena such as dark matter and dark energy and at last the mater-antimatter imbalance observed in the universe. This flaws found in the SM suggest the need for a more comprehensive theoretical framework that is able to tackle and answer these discrepancies found between theory and observation. SM constraints act as fuel, inspiring the search for new theories beyond the SM (BSM) and experiments aimed at discovering new physical phenomena.

Some of these BSM theories consist of extensions to the SM such as supersymmetric models or extradimensional theories [1].These novel BSM theories offer fresh insights and predictions regarding physical phenomena distinct from those of the SM [2]. An essential consideration in evaluating these theories is the degree of empirical support for their predictions.

In order to test these predictions, searches for new physics beyond the Standard Model (SM) are underway. Some of these searches take place at high-energy particle colliders, aiming to directly detect new processes or particles. Conversely, alternative search methods diverge from the traditional high-energy particle collider approach. These alternative approaches involve low-energy, high-precision experiments that measure quantities within the SM. New physics may be uncovered by observing deviations of these measured values from SM predictions. These low-energy phenomena are sensitive to new physics that manifest through the violation of fundamental symmetries such as P (parity), T (time reversal), and C (charge conjugation) [2]. Significant efforts have been dedicated to measuring and calculating these violations of fundamental symmetries in atoms and molecules [3, 2]. Part of these research on symmetry violations consists of investigations on nuclear-spin-dependent parity violating (NSD-PV) effects. These NSD-PV effects offer a means to investigate low-energy quantum chromodynamics and parity non-conservation (PNC) in nuclei [2, 4], they will be the main focus of this work.

These NSD-PV effects represent merely a fraction of the total PV effects observed in atoms, with the primary contributor remaining unaffected by nuclear spin [3] and rendering the detection of NSD-PV effects a challenging endeavor. Moreover, NSD-PV effects stem from various sources within atoms, posing a significant challenge in discerning the contribution of each source to the NSD-PV signal. A more detailed explanation of the broader PNC concept, as well as the specific NSD-PV effects, will be presented in the theory section. Nonetheless, the focus of interest in this study will center on the NSD-PV source coming from the nuclear anapole moment.

The concept of the anapole moment was introduced by Zel'dovich [5] in 1958, shortly following the discovery of parity violation [2]. He pointed out that in a system which has no definite parity, a special distribution of magnetic fields may arise [6, 7]. The anapole is a type of electromagnetic moment that does not consist on electric and magnetic monopoles, dipoles or quadruple moments [2, 6]. On the other hand, it consist of other multipole moments that are not treated in the multipole moment expansions normally. These terms of the multipole expansion are normally not treated as they give rise to contact potentials instead of long-range ones [2].

In a multipole expansion with classical charge and current distribution $\rho(\mathbf{r})$ and $\mathbf{j}(\mathbf{r})$, the electromagnetic scalar and vector potential $\Phi(\mathbf{r})$ and $\mathbf{A}(\mathbf{r})$ are written as a Taylor expansion around the source point $\mathbf{r}$ [7]. In the expansion of the vector potential the third term contains 8 independent components, the anapole moment being one of them [7]. By extracting the contribution of the anapole moment from the vector potential we can classically define the anapole moment as [8, 2]:

$$\mathbf{a} = -\pi \int r^2 \mathbf{j}(\mathbf{r}) d^3 r \tag{1}$$

The current distribution corresponding to this anapole moment $\mathbf{a}$ is that of a current winding. Figure 1 shows a depiction of such current distribution. This type of current winding gives a nonzero anapole moment due to the current in equation 1 being weighted by a factor r^2 [2].

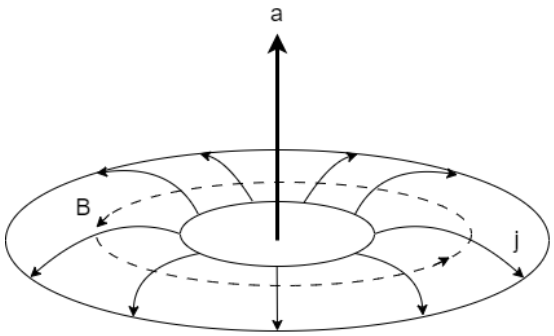

Figure 1: Diagram showing the toroidal current distribution $\mathbf{j}$ together with the magnetic field $\mathbf{B}$ and the anapole moment $\mathbf{a}$ that it generates.

The anapole moment $\mathbf{a}$ points along the direction of the nuclear spin $\boldsymbol{I}$ giving us the expression $\mathbf{a} = a\boldsymbol{I}/I$ [2]. The nuclear spin $\boldsymbol{I}$ is invariant under parity while the current term $\mathbf{j}$ in equation 1 is not and changes sign under coordinate inversion. This inconsistency in the behaviour of $\mathbf{a}$ under coordinate inversion means that the anapole moment violates parity but does not violate time reversal invariance.

The creation of this anapole moment comes from the PV weak interaction between nucleons inside the nucleus [2, 3]. These PNC nuclear forces create spin and magnetic helical strucures inside the nucleus [9] due to the P odd mixing of $s_{1/2}$ and $p_{1/2}$ states [6]. This helical structures give rise to the already mention toroidal current distribution shown in figure 1 [2]. The anapole moment then interacts with the atomic electrons via the magentic field generated by this toroidal current. As it was previously mentioned, the anapole term in the vector multipole expansion has the form of a contact potential. This means that the magnetic field of the anapole moment is only localized inside the doughnut in figure 1. The implication of this in atoms is that the electrons only interact with the nuclear anapole moment if the electron wave function penetrates inside the nucleus.

After the concept of the anapole was introduced many experiments were carried out with the goal of detecting this anapole moment but it was not until 1997 that the nuclear anapole moment was detected in the ^{133}Cs atom using atomic experiments [10]. This was the first and only observation of a nonzero nuclear anapole moment has been detected so far. In addition to experiments conducted on atoms, there are also proposed experiments involving molecules. This is due to research that has demonstrated that within diatomic molecules possessing $^2\Sigma_{1/2}$ and $^2\Pi_{1/2}$ electronic states, NSD-PV effects undergo significant enhancement, up to a factor of 10^5 [11, 12, 13]. Primarily attributable to the mixing of closely aligned rotational states with opposite parity [14, 4, 11, 13], including mixing of Λ and Ω doublets [14].

In order to measure the anapole moment in PNC experiments it is first crucial to precisely calculate the NSD P-odd interaction constant W_{PV}, known as the enhancement factor. This constant W_{PV} is calculated through numerical methods and it is necessary to establish a connection between experimental values and theory [13, 15]. A more extensive description of W_{PV} and how it connects to the NSD-PV effects will be given in the theory section. In any case, many calculations of W_{PV} have been performed with molecules. Most of these calculations have been carried in diatomic molecules due to the fact that NSD-PV effects are enhanced in them, however, also other works have proposed the use of linear triatomic molecules instead [16, 15]. Nonetheless, our focus in this work remains on the results acquired for diatomic molecules.

Although the number of diatomic molecules under study is quite extensive and keeps increasing, the types of molecules used follow a specific pattern. In all calculations the molecule under study consists of a heavy and a light atom, with the W_{PV} factor normally calculated for the heavy atom [13]. The heavy atoms is usually a metal and most of the types of groups of metals (transition metals, post-transition metals, alkaline earth, lanthanoids, actinoids...) in the periodic table have already been put the test [17, 13, 18, 19]. Although in some of these groups there are still lots of metallic elements that have not been studied yet.

Despite there being a wide range of metallic elements employed as the heavy atom in molecules, a review of the

literature revealed that this was not the case for the other light atom present in the molecules. It was notices that the most employed element for the light atom was fluorine, with most of the molecules studied being some type of metallic fluoride. Some exceptions where found and some nitrides, halides together with oxygen have also been utilized as the light atom [18]. Nonetheless, the most employed light atom in this types of calculation is fluorine [20, 21, 22, 23, 19, 24, 25].

As it was stated, most of the computations carried out in diatomic molecules tend to only focus on the W_{PV} parameter of the heavy element forming the molecule and not on that one of the lighter element. This is not surprising as the NSD-PV signal of the heavy atom is the dominant contribution to the NSD-PV signal of the whole molecule. However, performing a calculation of W_{PV} for both atoms in the molecule would allow for various PV effects to be disentangled from one another [15], giving a better understanding of the overall NSD-PV signal. Furthermore, calculating the enhancement factor W_{PV} for lighter atomic systems may allow to test nuclear theories that make predictions on such quantity.

In light of the reasons stated above, the primary objective of this study is to analyze and determine the W_{PV} value for the fluorine atom through ab initio calculations and explore its implications for the molecule as a whole. Initially, the W_{PV} value of fluorine will be computed for SrF, this molecule has already been studied in previous works but only the W_{PV} value of the Sr atom has been calculated. In the process we will vary various computational parameters in order to better understand how they affect the overall value of W_{PV}. Such computational parameters will be the type of basis set, the treatment of electron correlation, the number of correlated electrons, the virtual space cut-off, and the treatment of relativity. Notably, all these systems contain an open shell with one unpaired electron.

Subsequently, the W_{PV} value of fluorine for YF+ will be calculated. This system is isoelectronic to SrF but with the difference that in this case the molecule is a positive ion. Furthermore, two more lighter isoelectronic systems, CF and NF+ will also be studied. Studying these isoelectronic systems will provide a better understanding of how W_{PV} is influenced by the system's charge. Additionally, ions may offer experimental advantages due to their easier trapping, making them excellent candidates for NSD-PV experiments. At last the W_{PV} value of XeF will be computed.

2 Theory

In this section, we give an overview of the relevant theory describing PV (parity-violating) effects in atomic and molecular systems. The first subsection will provide an overview of the overall PV effects observed in these systems. Following this, subsequent sections will delve into a detailed examination of the two contributions to PV effects: nuclear spin-independent and spin-dependent (NSD) effects. Of particular interest in this study are the latter NSD contributions, given their significance in elucidating nuclear anapole moment effects.

2.1 PV Hamiltonian

Microscopically, atomic PV effects are caused by the weak interaction mediated by the exchange of a Z boson between atomic electrons and the nucleus [3, 2]. This Z boson interaction has a range of $\approx 2 \times 10^{-3}$ fm. In terms of atomic and molecular distances this range is a contact interaction. This contact interaction can be expressed in Hamiltonian form as [3]:

$$H_{PV} = \frac{G_F}{\sqrt{2}} \sum_q \left(C_q^{(1)} \bar{e} \gamma_\mu \gamma_5 e \bar{q} \gamma^\mu q + C_q^{(2)} \bar{e} \gamma_\mu e \bar{q} \gamma^\mu \gamma_5 q \right) \tag{2}$$

where $G_F \approx 1.435850 \times 10^{-62}\text{J}\cdot\text{m}^3 \approx 2.222516 \times 10^{-14} E_h \cdot a_b^3$[1] [4] is the Fermi constant, e and q are the electron and quark field operators respectively, $\gamma\mu$ and γ_5 are Dirac matrices and the summation is done over quark flavors $q = \{u, d, s, ...\}$.

The connection between the electron axial-vector currents and the quark vector currents ($\boldsymbol{A_e V_N}$) is expressed through the constants $C_q^{(1)}$, while the constant $C_q^{(2)}$ characterize the interaction of the electron vector currents with the quark axial-vector currents ($\boldsymbol{V_e A_N}$). This interaction constants describing the coupling to quarks can be combined to give the interaction constant for the the coupling to protons and neutrons in the nuclei [26, 3]:

$$C_p^{(1)} = 2C_u^{(1)} + C_d^{(1)} \tag{3}$$

$$C_n^{(1)} = 2C_d^{(1)} + C_u^{(1)} \tag{4}$$

$$C_p^{(2)} = -C_n^{(2)} = g_A C_p^{(1)} \tag{5}$$

where the value relating $C^{(1)}$ and $C^{(2)}$, $g_A \approx 1.26$, is the scale factor accounting for the partially conserved axial vector current [3]. These interactions constants can also be explicitly written in terms of the Weinberg angle θ_W [3, 15]:

$$C_p^{(1)} = \frac{1}{2}(1 - 4\sin^2\theta_W) \tag{6}$$

with the Weinberg angle giving the value $\sin^2\theta_W \approx 0.23$ [27].

Apart from the two terms given in equation 2, there are additional sources of PNC consisting of radiative corrections such as nuclear anapole moments and combined effects of Z-boson exchanged in combination with hyperfine interactions. This group of PNC sources consisting of radiative corrections are all NSD contributions.

Although there are several NSD-PV sources, in atomic PV experiments the main contributor to PV effects is spin independent. It is given by the interaction between electron axial vector and nucleon vector currents $\boldsymbol{A_e V_N}$. This interaction is described by the first term in equation 2. This spin independent interaction can be simplified[2] to an interaction in the electron sector with the following expression [3]:

$$H_W = Q_W \frac{G_F}{\sqrt{8}} \gamma_5 \rho(r) \tag{7}$$

where $\rho(x)$ is the nuclear density and Q_W is the nuclear weak charge.

[1] where E_h is the Hartree energy and a_b is the Bohr radius.

[2] protons and neutrons are approximated as non relativistic and are assumed to have equal densities and distributions inside the nucleus.

2.2 Nuclear Spin Dependent Effects

Apart from the NSD radiative corrections mentioned in the previous section, there is one more source of NSD-PV still to be referred to. That one being the second term in equation 2, the interaction between electron vector currents and nucleon axial vector currents $\boldsymbol{V_e A_N}$. All these spin NSD-PV effects can be combined to form an NSD-PV interaction term in the electronic Hamiltonian of the following form [15, 4]:

$$H_{NSD} = \frac{G_F}{\sqrt{2}I} \sum_i \left(\kappa_{ax} + \kappa_{hfs} + \kappa_A\right) (\boldsymbol{\alpha} \cdot \boldsymbol{I})\, \rho(\boldsymbol{r}) \tag{8}$$

First thing to be notice is that the Hamiltonian is formed out of three terms, each corresponding to one of the NSD sources. This NSD terms have as a common factor a product formed firstly by the Fermi weak interaction coupling constant G_F, the Dirac matrices in the standard representation $\boldsymbol{\alpha}$, the nuclear spin $\boldsymbol{I}$ and the nuclear density distribution $\rho(\boldsymbol{r})$ with $\boldsymbol{r}$ being the electronic coordinates.

The three NSD terms are represented by the dimensionless constants κ_A, κ_{ax} and κ_{hfs}, they describe the strength of each of the sources of the PNC [7]. The first parameter κ_{ax} comes from the already mentioned electroweak neutral coupling between the electron vector and nucleon axial-vector currents $\boldsymbol{V_e A_N}$, the next term κ_{hfs} is due to the nuclear-spin-independent weak interaction $\boldsymbol{A_e V_N}$ combined with the hyperfine interaction, and the last contribution κ_A arises from the nuclear anapole moment interaction.

Each of these terms κ has its own expression that describes its behavior in more detail. For κ_{ax} the expression is given by the following equation [3, 18, 15] in nuclear shell model form:

$$\kappa_{ax} = -C_N^{(2)} \frac{K - 1/2}{I + 1} \tag{9}$$

In the equation above $C_N^{(2)}$ is the weak interaction constant introduced in the second term of the overall PV Hamiltonian and it varies in value depending whether the unpaired nucleon is a proton or a nucleon, $N = n, p$. The value K is the relativistic angular quantum number for the unpaired nucleon [3], it is given by $K = (I + 1/2)(-1)^{I - l_i + 1/2}$ where l_i is the orbital angular momentum of the external unpaired nucleon.

The second term κ_{hfs} is described by [15, 9]:

$$\kappa_{hfs} = -\frac{1}{3} Q_W \frac{\alpha \mu}{m_p r_0 A^{1/3}} \tag{10}$$

$$\approx 2.5 \times 10^{-4} A^{2/3} \mu_i \tag{11}$$

where we have the nuclear weak charge Q_W, the fine structure constant $\alpha \approx 1/137$, the proton mass m_p, the scale of the nuclear radius $r_0 \approx 1.2$ fm, μ_i is the nucleon magnetic moment in nuclear magnetons[3] and A is the mass number. The last term corresponding to the nuclear anapole moment will be explained in the following section.

2.2.1 Nuclear Anapole Moment

The nuclear anapole moment term κ_A originates due to the second-order multipole expansion of the magnetic vector-potential together with the P– and T– violating static magnetic quadrupole moments [7]. In a valence nucleon model the coupling parameter to the anapole moment can be expressed as follows [9, 13, 6]:

$$\kappa_A = \frac{1}{10} \frac{\alpha \mu_i}{m_p r_0} g_i A^{2/3} \frac{K}{I + 1} \tag{12}$$

$$\approx 1.15 \times 10^{-3} g_i \mu_i A^{2/3} \frac{K}{I + 1} \tag{13}$$

All the terms used in this equation have been presented already except for the dimensionless constant g_i that characterizes the nucleon-nucleus weak potential. This dimensionless constant is poorly known and lots of different

[3] For protons $\mu_p \approx 2.793$[28, 29], for neutrons $\mu_n \approx -1.913$[28, 29].

values are available in the literature, a summary of these values can be found in [30]. In this work the values used for g_i will be the ones also used in [15] where for protons $g_p \approx 3.4 \pm 0.8$ and for neutrons $g_n \approx 0.9 \pm 0.6$. The central values will be used, that is $g_p = 3.4$ and $g_n = 0.9$.

One thing to notice is that due to the $A^{2/3}$ term, there is a scaling effect proportional to the nucleon number. For the term corresponding to κ_{ax} there is no dependence on the nucleon number, however for κ_{hfs} the mass number is also present. Although both κ_A and κ_{hfs} scale with the nucleon number to the same power, due to a small numerical prefactor present in κ_{hfs} its contribution is strongly suppressed in comparison to the one given by κ_A. This means that in systems containing heavy nuclei with a large nucleon number the nuclear anapole moment can provide the dominant contribution to the NSD-PV. However, in this study, the atom of interest is fluorine (F), which has a relatively low atomic number. Therefore, it cannot be assumed that the nuclear anapole dominates the NSD-PV signal in this atom. It is essential to consider that all sources of NSD-PV contribute to the overall signal on equal footing.

2.3 First-order Perturbation on Model Hamiltonian

In molecular systems with non zero nuclear spin and with $^2\Sigma_{1/2}$ and $^2\Pi_{1/2}$ electronic states, equation 8 can be rewritten as an effective operator that is added to the spin-rotational Hamiltonian [13, 31, 15]:

$$H_{NSD}^{eff} = \kappa W_{PV}(\hat{\boldsymbol{n}} \times \boldsymbol{S}_{eff}) \cdot \boldsymbol{I}/I \tag{14}$$

The terms in bold are the following, $\hat{\boldsymbol{n}}$ is the unit vector pointing from the heavier to the lighter nucleus parallel to the internuclear axis, $\boldsymbol{S_{eff}}$ is the effective spin of the valence electron and the dimensionless constant is $\kappa = (\kappa_A + \kappa_{ax} + \kappa_{hfs})$. Finally, the term W_{PV} represents the overlap of the unpaired electron with the nucleus [16] and it is the value of interest in this work.

In heavy enough atoms where κ is dominated by κ_A, the signal of the anpole moment can be isolated. This leads to equation 14 describing the interaction of the valence atomic electron with the nuclear anapole moment inside the nucleus. When this happens we can rename W_{PV} as W_A but as it was previously mentioned this is not the case for F.

For this effective coupling constant κ to be experimentally determined it is crucial to calculate the value of the W_{PV} parameter with high accuracy [15]. This parameter depends on the electronic structure of the system in question and can be found from evaluating the $\boldsymbol{\alpha}\rho(\boldsymbol{r})$ term in the molecular spinor basis [13]. The two open shell electronic states of interest ($^2\Sigma_{1/2}$, $^2\Pi_{1/2}$) are both twofold degenerate which correspond to the two possible projections of the electronic angular momentum along the internuclear axis $\hat{\boldsymbol{n}}$, i.e., $|\Omega\rangle = |\pm 1/2\rangle$ [13, 4]. Operating in this twofold degenerate state means that the operator $\frac{G_F}{\sqrt{2}}\boldsymbol{\alpha}\rho(\boldsymbol{r})$ is equivalent to $W_{PV}(\hat{\boldsymbol{n}} \times \boldsymbol{S_{eff}})$ giving the form in equation 14 [13].

This leads the parameter W_{PV} to be defined from the operator term $\boldsymbol{\alpha}\rho(\boldsymbol{r})$ in equation 8 as the transition element between the two different states $|\Omega\rangle$ [32, 31, 15, 4]:

$$W_{PV} = \frac{G_F}{\sqrt{2}} \langle +1/2| \sum_i \rho(\boldsymbol{r}_i)\alpha_+ |-1/2\rangle \tag{15}$$

where

$$\alpha_+ = \alpha_x + i\alpha_y = \begin{pmatrix} 0 & \sigma_x \\ \sigma_x & 0 \end{pmatrix} + i \begin{pmatrix} 0 & \sigma_y \\ \sigma_y & 0 \end{pmatrix} \tag{16}$$

with σ_x and σ_y being the Pauli matrices. In conclusion, the parameter W_A can be defined as the amplitude of the expectation value of the mixed parity state $|\Omega\rangle = |\pm 1/2\rangle$.

2.3.1 Finite Field Method

The approach employed to calculate the W_{PV} parameter in this study is the finite field method. In this technique, perturbation theory is utilized, and the total Hamiltonian is modeled as a function comprising an unperturbed Hamiltonian H_0 and a first-order perturbation term. The perturbation term is modelled as the NSD-PV Hamiltonian

given in the form of equation 15 along with a perturbation parameter λ. This parameter λ describes the strength of the effective NSD-PV effect for the nucleus [15]:

$$H(\lambda) = H_0 + \lambda \frac{G_F}{\sqrt{2}} \sum_i \rho(\boldsymbol{r}_i)\alpha_+ \tag{17}$$

In this work the unperturbed Hamiltonian consist of the Dirac-Coulomb Hamiltonian given by [4]:

$$H_0 = \sum_i^n [\beta_i mc^2 + c\boldsymbol{\alpha}_i \cdot \hat{\boldsymbol{p}}_i - V_{eN}(r_i)] + \sum_{i<j}^n \frac{1}{r_{ij}} \tag{18}$$

where $\boldsymbol{\alpha}_i$ and β are Dirac matrices, V_{eN} is the nuclear Coulomb potential, r_i is the distance of electron i to the nucleus and r_{ij} is the distance between electron i and electron j. The finite size of the nucleus is taken in to account by modelling the Coulomb potential V_{eN} as a Gaussian charge distribution [4, 33]. In any case, going back to equation 17, for small values of λ the total energy of the Hamiltonian can be expanded as a Taylor series around $\lambda = 0$:

$$E(\lambda) = E(0) + \lambda \frac{dE(\lambda)}{d\lambda}\bigg|_{\lambda=0} + ... \tag{19}$$

The perturbation strength λ must be small enough to ensure that the calculation remains within the linear regime while also being sufficiently large to prevent the loss of precision in the total energy change. Operating within the linear domain permits the neglect of higher-order terms in equation 19. Consequently, according to the Hellmann-Feynman theorem, W_A can be numerically obtained from the first derivative of the energy with respect to λ [4, 15]:

$$W_{PV} = \frac{dE(\lambda)}{d\lambda}\bigg|_{\lambda=0} \tag{20}$$

When running the calculation, it is essential to test the linearity of the expression above to determine the correct perturbation strength λ. To achieve this, the strength of the linear relationship between the energy and λ is quantified using the correlation coefficient[4] r. This r coefficient is computed using the `stats.linregress` command from the SciPy package in Python. By examining the r coefficient for different values of λ it was established that the best linear fit was obtained for perturbation strengths of the order of $\sim 10^{-6}$ and $\sim 10^{-7}$.

[4]It ranges from 1 to -1, indicating whether the relationship is positive or negative. An r value of 0 means there is no correlation between the variables, while values close to 1 or -1 indicate a strong linear relationship.

3 Computational Methods and Considerations

Solving the full Dirac or Schrödinger equation will yield the exact solution for the energy of the system but unfortunately solving such equation for systems like molecules is too computationally costly. This means some approximations have to be made, the results will yield a lower accuracy but in return the computational cost and time will be reduced. In this research all calculations will be carried out with the relativistic ab initio quantum chemistry DIRAC19 software. This program is capable of calculating various molecular properties using the Dirac-Hartree–Fock (HF), Møller–Plesset perturbation theory (MP2), density functional theory (DFT), configuration interaction (CI) and coupled cluster (CC) electronic structure theories. In this work only HF, CC and MP2 methods will be explained, the derivation of these types of methods will be looked in detail in the Computational Methods section 3.3.

3.1 Born-Oppenheimer Approximation

The general expression for a molecular Hamiltonian has the following form [34]:

$$\hat{H}_{mol} = \hat{T}_e(\boldsymbol{r}) + \hat{T}_N(\boldsymbol{R}) + V_{Ne}(\boldsymbol{r}, \boldsymbol{R}) + V_{ee}(\boldsymbol{r}) + V_{NN}(\boldsymbol{R}) \tag{21}$$

Where the $\hat{T}$ operators are the kinetic terms for the electrons and nuclei in the molecule respectively, V_{Ne} is the attraction potential between nuclei and electrons and the last two potential terms correspond the repulsion between electrons (V_{ee}) and the repulsion between nuclei (V_{NN}). All these terms are functions dependent either on electronic coordinates $\boldsymbol{r}$ or nuclear coordinates $\boldsymbol{R}$. Now our goal is to solve the Schrödinger equation for this Hamiltonian ($\hat{H}_{mol}\Psi = E_{mol}\Psi$) but a problem arises if we do this. The Schrödinger equation can only be solved exactly for the hydrogen atom [35], anything more complex can only be solved using an approximation. This approximation is the Born-Oppenheimer (BO) approximation and is based on the fact that electrons are thousands of time lighter than nuclei. This means electrons move much faster than their nuclear counterparts and so from their perspective it seems like the nuclei are static and do not change their spatial coordinates. Now, how does this help in solving the Schrödinger equation?

In quantum mechanics, if the Hamiltonian can be separated as a sum of terms each depending on different variables ($\hat{H} = \hat{H}_1(\boldsymbol{r_1}) + \hat{H}_2(\boldsymbol{r_2})$) then the wavefuntion can be expressed as a product of functions with different variables ($\Psi = \psi_1(\boldsymbol{r_1})\psi_2(\boldsymbol{r_2})$). If the molecular Hamiltonian could be expressed as a sum of nuclear and electronic Hamiltonians, then the molecular wavefunction would consist of a product of two separate functions:

$$\hat{H}_{mol}\Psi = E_{mol}\Psi \rightarrow \left[\hat{H}_e(\boldsymbol{r}) + \hat{H}_N(\boldsymbol{R})\right]\psi_e(\boldsymbol{r})\psi_N(\boldsymbol{R}) = E_{mol}\psi_e(\boldsymbol{r})\psi_N(\boldsymbol{R}) \tag{22}$$

Now there is a problem with the Hamiltonian in equation 21, it does not satisfy the condition for a Hamiltonian consisting on separable Hamiltonians because the term for the electron-nucleus attraction V_{Ne} depends both on $\boldsymbol{r}$ and $\boldsymbol{R}$ [34]. Here is where the BO approximation comes in to play. Treating the nuclei as being static in the electrons frame will allow for the wavefunction to be expressed in a similar form to the one previously mentioned:

$$\Psi = \psi_e(\boldsymbol{r;R})\psi_N(\boldsymbol{R}) \tag{23}$$

where the ; symbol in the argument of the electronic part means that we are treating the nuclear coordinates no longer as a variable but as a parameter that is fixed. This type of separation allows us to separate as well the Hamiltonian in the following way:

$$\hat{H}_{mol} = \overbrace{\hat{T}_e(\boldsymbol{r}) + V_{Ne}(\boldsymbol{r;R}) + V_{ee}(\boldsymbol{r})}^{\hat{H}_e} + \overbrace{V_{NN}(\boldsymbol{R}) + \hat{T}_N(\boldsymbol{R})}^{\hat{H}_N} = \hat{H}_e + \hat{H}_N \tag{24}$$

Then we know that the electronic Hamiltonian will give the electronic energies if we solve the electronic Schrödinger equation:

$$\hat{H}_e\psi_e(\boldsymbol{r;R}) = E_e(\boldsymbol{R})\psi_e(\boldsymbol{r;R}) \tag{25}$$

where the electronic energy depends on the parameter $\boldsymbol{R}$. Then if we solve for the total molecular energy we obtain the following expression:

$$E_{mol} = \langle \Psi | \hat{H}_{mol} | \Psi \rangle = E_e + \frac{\hat{H}_N \psi_N(\boldsymbol{R})}{\psi_N(\boldsymbol{R})} \tag{26}$$

It most be noticed that in this derivation of the molecular energy expression, the action of the nuclear kinetic term $\hat{T}_N$ on the electronic part of the wavefunction vanishes due to the BO approximation. This is because $\hat{T}_N$ is an operator that applies differentiation with respect to the nuclear coordinates $\boldsymbol{R}$ and our electronic wavefunction treats $\boldsymbol{R}$ as a parameter that remains fixed[5]. Knowing this, the nuclear Schrödinger equation can be written:

$$\overbrace{\left(\hat{T}_N(\boldsymbol{R}) + V_{NN}(\boldsymbol{R}) + E_e(\boldsymbol{R})\right)}^{\hat{T}_N(\boldsymbol{R})+U(\boldsymbol{R})} \psi_N(\boldsymbol{R}) = E_{mol}\psi_N(\boldsymbol{R}) \quad ; \quad U(\boldsymbol{R}) = V_{NN}(\boldsymbol{R}) + E_e(\boldsymbol{R}) \tag{27}$$

The new term $U(\boldsymbol{R})$ is known as the internuclear potential for a given $\boldsymbol{R}$ [34]. This internuclear potential can be expressed in Hamiltonian form as [36]:

$$\hat{H} = \sum_i \hat{h}(i) + \frac{1}{2}\sum_{i \neq j} \hat{g}(i,j) + V_{NN} \quad ; \quad V_{NN} = \frac{1}{2}\sum_{A \neq B} \frac{Z_A Z_B}{R_{AB}} \tag{28}$$

where this time the Hamiltonian is expressed in terms of one-electron and two-electron operators, ($\hat{h}(i)$ and $\hat{g}(i,j)$ respectively). The one-electron operator will contain the kinetic term of the electron and the electron-nucleus interaction. The two-electron operator represents the electron-electron repulsion interaction term. Even though the nuclear kinetic term is neglected, the BO approximation still takes in to account the variation in the position of the nuclei when determining the electronic energy. This contribution comes from the V_{NN} term in equation 28.

3.1.1 One-Electron Operator

The form of the Hamiltonian in the BO approximation can vary depending on the type of one-electron operator chosen for the calculation. In the non-relativistic framework the one-electron operator is a one component (1c) scalar. On the other hand, in the relativistic regime the expression for the energy of a relativistic free particle gives both positive and negative energy solutions [37], implying the existence of both particles and antiparticle [38]. This results in the one-electron operator becoming a four component (4c) operator describing both particle and antiparticle with their corresponding spins included.

The 4c Hamiltonian can be computationally too heavy for big systems containing many electrons. The antiparticle part of the Hamiltonian can be frozen in order to obtain a two component Hamiltonian (2c), where the spin-orbit interaction between the spin of the electron and the magnetic field originating from the nuclear motion in the electrons frame is well described. Nonetheless, the 4c operator will still give the most accurate results for relativistic effects. In order to reduce computational costs, new types of Hamiltonian like the exact two component Hamiltonian (X2c)[6] have been developed. The DIRAC program will work by default with 4c Hamiltonian, nonetheless, 2 component approximation (X2c) and non relativistic Hamiltonians can also be implemented [39].

In equation 28 the one-electron operator is split in to a relativistic free-electron Dirac Hamiltonian $\hat{h}^{(0)}$ and an electric potential V_{eN} addressing the electron-nucleus interaction [39]:

$$\hat{h}_D = \hat{h}^{(0)} + V_{eN} = \beta mc^2 + c\,(\boldsymbol{\alpha} \cdot \hat{\boldsymbol{p}}) + V_{eN} \tag{29}$$

In the non-relativistic case the free-electron Hamiltonian only contains a kinetic term but in the relativistic regime a mass term is added aswell. In general $\hat{h}_D$ is the Dirac-Hamiltonian in a bare nuclear field [36].

[5] Differentiation with respect to a constant always yields zero so in this case $\nabla_N^2(\boldsymbol{R})\psi_e(\boldsymbol{r};\boldsymbol{R}) \approx 0$.

[6] This Hamiltonian yields the same results as the 4c Hamiltonian for for positive energy solutions[37]

3.1.2 Two-Electron Operator

For the non-relativistic case the two-electron operator $\hat{g}(i,j)$ has the form:

$$\hat{g}^{Coulomb}(i,j) = \frac{1}{r_{ij}} \tag{30}$$

When using this approximation one can notice that we obtain the previously mentioned Dirac-Coulomb Hamiltonian in equation 18 [37]. However, this means that the Dirac-Coulomb Hamiltonian is not fully relativistic as it considers the Coulomb interaction to be instantaneous. In order to obtain the full relativistic picture, the two-electron operator has to be modified so it includes magnetic interactions as well as retardation effects. In order to obtain the two-electron operator in the relativistic framework, a Taylor expansion around c^{-1} up to c^{-2} is performed [40]. The instantaneous Coulomb-interaction is then the zeroth-order term of the expansion and first-order correction to the overall Coulomb interaction is given by the Breit term [37]:

$$\hat{g}^{Breit}(i,j) = -\frac{c\boldsymbol{\alpha}_i \cdot c\boldsymbol{\alpha}_j}{2c^2 r_{ij}} - \frac{(c\boldsymbol{\alpha}_i \cdot \mathbf{r_{ij}})(c\boldsymbol{\alpha}_j \cdot \mathbf{r}_{ij})}{2c^2 r_{ij}^3} \tag{31}$$

The Breit term can be rearranged and split in to two terms, the Gaunt term and the gauge term [36]:

$$\hat{g}^{Breit}(i,j) = \hat{g}^{Gaunt}(i,j) + \hat{g}^{gauge}(i,j) = -\frac{c\boldsymbol{\alpha}_i \cdot c\boldsymbol{\alpha}_j}{c^2 r_{ij}} - \frac{(c\boldsymbol{\alpha}_i \cdot \nabla_i)(c\boldsymbol{\alpha}_j \cdot \nabla_j) r_{ij}}{2c^2} \tag{32}$$

So the expression for the total relativistic Coulomb interaction is give by:

$$\begin{aligned} \hat{g}(i,j) &= \hat{g}^{Coulomb}(i,j) + \hat{g}^{Breit}(i,j) \\ &= \hat{g}^{Coulomb}(i,j) + \hat{g}^{Gaunt}(i,j) + \hat{g}^{gauge}(i,j) \\ &= \frac{1_{4\times4}}{r_{ij}} - \frac{c\boldsymbol{\alpha}_i \cdot c\boldsymbol{\alpha}_j}{c^2 r_{ij}} - \frac{(c\boldsymbol{\alpha}_i \cdot \nabla_i)(c\boldsymbol{\alpha}_j \cdot \nabla_j) r_{ij}}{2c^2} \end{aligned} \tag{33}$$

where the overall expression consists of a charge–charge interaction $\hat{g}^{Coulomb}$, a current–current interaction $\hat{g}^{Gaunt}$ and a gauge term $\hat{g}^{gauge}$ [36, 37]. Even though the Coulomb term is in non-relativistic form, it describes also the spin–same orbit interaction. The Gaunt term describes the spin–other-orbit as well as orbit–orbit and spin–spin interactions. The gauge term contributes only to the spin-free (scalar) interaction and is usually less relevant. The Gaunt term is a magnetic interaction (spin) while the other terms represents retardation effects[40].

3.2 Molecular Orbital Theory

Molecular Orbital theory (MO) is widely used for describing the electronic structure of molecules. Unlike Valence Bond theory, MO theory does not assign electrons to specific chemical bonds within the molecule. Instead, each electron is influenced by all atomic nuclei in the molecule to varying degrees. Molecular orbitals are constructed as linear combinations of atomic orbitals belonging to the atoms forming the molecule (LCAO-MO) [35]:

$$\psi = \sum_{A}^{N} c_A \Phi_A \tag{34}$$

where ψ is the molecular orbital, $\boldsymbol{\phi}$ is the atomic orbital and c_A is the linear coefficient assigned to the atomic orbitsl $\boldsymbol{\phi_A}$.

3.2.1 Basis Sets

In order to describe this molecular orbitals first the atomic orbitals have to be specified. The general expression for an atomic orbital is give by the expression:

$$\Phi_{nlm}(r,\theta,\phi) = R_n(r) Y_{lm}(\theta,\phi) \tag{35}$$

where the atomic orbital is divided in two parts, the radial part $R_n(r)$ and the angular part $Y_{lm}(\theta, \phi)$. The radial part can be described by basis functions, the combination of these basis functions will form a basis set. Basis functions can be divided in two types, Slater type orbitals (STO) and Gaussian type orbitals (GTO) [41]:

$$\Phi_{abc}^{STO}(x, y, z) = Nx^a y^b z^c e^{-\zeta r}, \qquad \Phi_{abc}^{GTO}(x, y, z) = Nx^a y^b z^c e^{-\zeta r^2} \tag{36}$$

they are given in Cartesian coordinates. N is a normalization constant and a, b, c control angular momentum ($L = a+b+c$). The parameter ζ controls the width of the orbital (large ζ gives tight function, small ζ gives diffuse function) [41] and at last $r = \sqrt{x^2 + y^2 + z^2}$. The use of L for the specification of the angular momentum instead of spherical harmonics is justified because using spherical harmonics is in computational terms too complicated. Both STO and GTO have similar form, only differing in the argument of the exponent. The STO gives a more accurate description of the actual orbital than the GTO but it is computationally more demanding. A solution to this problem is to use a linear combination of GTOs to emulate the behaviour of an STO. This technique will be less computationally heavy and it will give a good approximation of the STO. This linear combination of GTOs is defined as a contracted Gaussian type orbital (CGTO), where the terms in the linear combination are now called primitive Gaussian type orbitals (PGTO):

$$\Phi_{abc}^{CGTO} = N \sum_{j=1}^{K} c_j x^a y^b z^c e^{-\zeta_j r^2} \tag{37}$$

where K is the number of PGTOs per CGTO. A combination of n PGTOs used to mimic an STO is called "STO-nG". The larger the number of PGTO, the more it will resemble the actual STO. In figure 2 the quality of the STO-nG functions is shown for varying n, it is clear that a larger number of PGTO in a CGTO will give a more precise description of the STO

If only one basis function (STO, GTO or CGTO) is used in the description of each atomic orbital then the basis set is called a minimal basis set. When two basis functions are used for the atomic orbital then it is called a double zeta (Dz) basis sets and three basis functions per atomic orbital is a triple zeta (Tz) basis set. This can be extrapolated to a larger number of basis set (quadruple, quintuple etc.). The number of basis functions used per orbital gives the cardinality of the basis set. A larger basis set increases both the accuracy and the computational cost of the calculation. For an infinite number of basis functions per atomic orbital, the basis set is said to be a complete basis set (CBS).

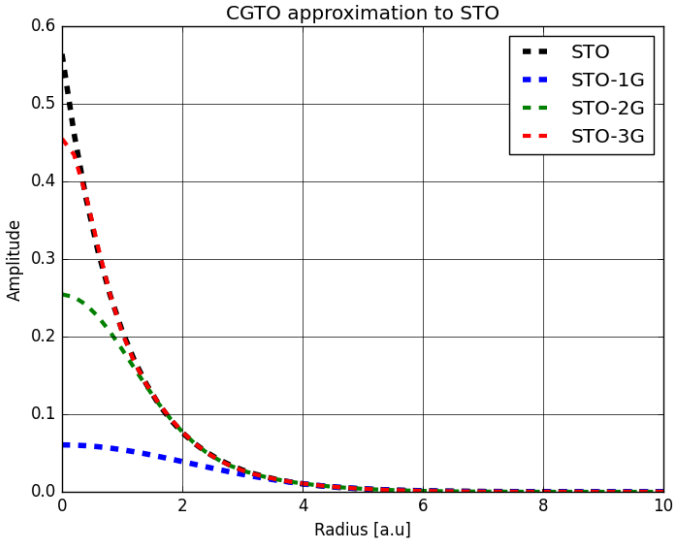

Figure 2: Comparison of the quality of the STO obtained from CGTO at the STO-1G, STO-2G, STO-3G level. The equation used for the CGTOs is given in radial form instead of using the Cartesian format given in equation 37. The values for the coefficients c_j and the parameters ζ are given in [42].

Other variations of basis sets can be used like split valence basis sets (vXz) which use a minimal basis for core orbitals and a larger basis for valence orbitals [41]. In this basis sets the X specifies the cardinality of the basis.

Depending on the system under study, either tight or diffuse basis functions can be employed to achieve a more accurate description. Tight functions have high values for ζ and accurately represent the orbital's behavior near the nucleus. In contrast, diffuse functions have lower ζ values and decay more slowly than tight functions. These types of functions enhance the quality of the atomic orbital description in the outer regions, making them particularly useful in systems where electrons are located far from the nucleus, such as anions[7].

3.2.2 Dyall Basis Sets

The types of basis sets discussed in the previous section were designed to give good results and convergence for HF methods but they are not suitable for post-Hartree-Fock calculation where electron correlation is taken in to account [41]. In order to solve this problem, Dunning developed the correlation consistent basis sets which are labelled cc-pVXZ. The "cc-" in front stands for correlation consistent and the letter p stands for the addition of polarization functions.

Polarization functions describe how an atomic orbital behaves when another atom approaches. The electric field of the approaching atom can induce a shift in the electron density of the orbital being influenced. For instance, if an s orbital is approached by an atom that repels electrons, the electron density within the spherical s orbital will redistribute away from the approaching atom. Consequently, the resulting electron density may resemble more closely the shape of a p orbital rather than a symmetric s orbital, indicating polarization.

Polarization functions address this phenomenon by incorporating higher-order angular momentum functions into the existing orbital basis set. This addition allows for a more accurate representation of electron correlation and polarization effects.

In the DIRAC program there is a wide variety of GTOs available for use, where the main ones are the ones developed by Dyall and coworkers. This type of basis sets follow the correlation consistent methodology introduced by Dunning. Dyall basis sets include electron correlation functions for valence, outer core and inner core orbitals. They add as well diffuse functions [43] for s, p and d block elements [39]. The main characteristic of the Dyall basis sets is that they are designed to be suitable for relativistic calculations.

The relativistic Hamiltonian 29 is a four component Hamiltonian that requires a four component spinor on which to act. This four component spinor is normally represented as two component object:

$$\Psi = \begin{pmatrix} \psi^L \\ \psi^S \end{pmatrix} \tag{38}$$

where each of the components is a two component object itself. The values ψ^L and ψ^S are the large and small components of the four component spinor respectively. The large component would stand for the positive energy solutions and the small component for the negative energy solutions. This components can be expressed in terms of each other and for an electron in a hydrogen like atom the small component can be expressed in terms of the large component as follows [44]:

$$\psi^S = \left(2mc^2 + \epsilon - V\right)^{-1} c\boldsymbol{\sigma}\hat{\boldsymbol{p}}\psi^L \tag{39}$$

where V is the potential, ϵ the eigenvalue and $\hat{\boldsymbol{p}}$ is the momentum. Any basis set used to resolve the four component Dirac Hamiltonian must satisfy this coupling for the coupling between small and large component. When this coupling is taken to the non-relativistic limit for positive energy orbitals then we obtain what is called as kinetic balance [39]. This means that the small and big components of the basis sets must satisfy the following relation [44]:

$$\chi^S = \frac{1}{2mc}\boldsymbol{\sigma}\hat{\boldsymbol{p}}\chi^L \tag{40}$$

[7] Anions are negatively charged ions.

3.3 Computational Methods

3.3.1 Hartree-Fock

Hartree-Fock (HF) theory posits that each electron's motion can be described by a single-particle function (orbital), which does not explicitly depend on the instantaneous motions of the other electrons. Instead, each electron interacts with an average charge distribution formed by all other electrons. This method belongs to the category of variational methods[8] and derives a set of N-coupled equations for the N spin orbitals. Solving these equations yields the HF wave function and energy of the system.

The following derivation of HF theory will follow the notes provided by David Sherrill [45], using Hartree atomic units ($\hbar = e = a_0 = m_e = 1$) in subsequent sections. The objective of this method is to solve the electronic Schrödinger equation resulting from the time-independent Schrödinger equation (non-relativistic case) under the Born-Oppenheimer approximation:

$$\hat{H}_{el}^{NR}|\Psi(\boldsymbol{r},\boldsymbol{R})\rangle = \left[-\frac{1}{2}\sum_{i}^{n}\nabla_i^2 - \sum_{A,i}^{N,n}\frac{Z_A}{r_{Ai}} + \sum_{A>B}^{N}\frac{Z_A Z_B}{R_{AB}} + \sum_{i>j}^{n}\frac{1}{r_{ij}}\right]|\Psi(\boldsymbol{r},\boldsymbol{R})\rangle = E_{el}|\Psi(\boldsymbol{r},\boldsymbol{R})\rangle \tag{41}$$

where $|\Psi(\boldsymbol{r},\boldsymbol{R})\rangle$ is the electronic wave function depending on the electronic and nuclear coordinates ($\boldsymbol{r}$ and $\boldsymbol{R}$ respectively). Furthermore, N is the total number of nuclei, n is the total number of electrons, Z_X is the atomic number of nuclei X, r_{Ai} is the distance between nuclei A and electron i, r_{ij} is distance between electrons i and j and at last R_{AB} is the distance between nuclei A and B. Another way of expressing this equation is in term of kinetic and potential terms:

$$\left[\hat{T}_e(\boldsymbol{r}) + \hat{V}_{eN}(\boldsymbol{r},\boldsymbol{R}) + \hat{V}_{NN}(\boldsymbol{R}) + \hat{V}_{ee}(\boldsymbol{r})\right]|\Psi(\boldsymbol{r},\boldsymbol{R})\rangle = E_{el}|\Psi(\boldsymbol{r},\boldsymbol{R})\rangle \tag{42}$$

As we are making use of the BO approximation, it is possible to rewrite equation 41 in terms of one and two electron operators like in equation 28:

$$\hat{H}_{el}^{NR} = \sum_{i}^{n}\hat{h}(i) + \frac{1}{2}\sum_{i<j}^{n}\hat{g}(i,j) + V_{NN} \tag{43}$$

where the one-electron operator has the form:

$$\hat{h}(i) = -\frac{1}{2}\nabla_i^2 - \sum_{A}^{N}\frac{Z_A}{r_{Ai}} \tag{44}$$

In this case the one-electron operator does not have a mass term like equation 29 and the two-electron operator does not contain any of the Breit terms. This is due to the fact that we are treating the BO approximation in the non-relativistic case for this derivation.

In the HF method, a first approximation to the wavefunction is done by assuming that the electrons in the system do not interact with each other. In this case the overall wavefunction can be separated and treated as the product of all spin-orbitals involved in the system:

$$\Psi_{HP}(\boldsymbol{x_1},\boldsymbol{x_2},...,\boldsymbol{x_n}) = \chi_1(\boldsymbol{x_1})\chi_2(\boldsymbol{x_2})\ldots\chi_n(\boldsymbol{x_n}) \tag{45}$$

this type of wavefunction is the Hartree product. The spin-orbital for electron i is $\chi_i(\boldsymbol{x_i})$ and is dependent on $\boldsymbol{x}$ which is the set of spin-space coordinates with the form $\boldsymbol{x} = \{\boldsymbol{r}, w\}$. The spin-space coordinates are formed from combining spatial coordinates $\boldsymbol{r}$ with generic spin coordinates w ($w = \alpha$ for spin up and $w = \beta$ for spin down). So the spin-orbitals usually can be expressed as a product of a spatial orbital with a spin function, $\chi(\boldsymbol{x}) = \phi(\boldsymbol{r})\alpha(w)$.

[8] Variational methods are based on the variational principle, which states that the energy calculated using any arbitrary trial wavefunction is never less than the true energy. This implies that by varying the coefficients in the trial wavefunction to minimize the energy, the resulting coefficients provide the best approximation for that particular form of trial function [35].

This type of wavefunction does not satisfy *Pauli's antisymmetry principle* which states that a wavefunction describing fermions should be antisymmetric when interchanging any set of space-spin coordinates [46]. This shortcoming can be solved by using the linear combination of spin-orbitals given by the Slater determinant. For n spin-orbitals the Slater determinant has the form:

$$\Psi = \frac{1}{\sqrt{n!}} \begin{vmatrix} \chi_1(\boldsymbol{x_1}) & \chi_2(\boldsymbol{x_1}) & \cdots & \chi_n(\boldsymbol{x_1}) \\ \chi_1(\boldsymbol{x_2}) & \chi_2(\boldsymbol{x_2}) & \cdots & \chi_n(\boldsymbol{x_2}) \\ \vdots & \vdots & \ddots & \vdots \\ \chi_1(\boldsymbol{x_n}) & \chi_2(\boldsymbol{x_n}) & \cdots & \chi_n(\boldsymbol{x_n}) \end{vmatrix} = |12\ldots n\rangle \tag{46}$$

Now that the form for the Hamiltonian and of the wavefunction are known, the total energy of the system can be found by:

$$E_{HF} = \langle\Psi|\hat{H}_{el}^{NR}|\Psi\rangle = \sum_i \langle i|\hat{h}|i\rangle + \frac{1}{2}\sum_{ij}\left([ii|jj] - [ij|ji]\right) \tag{47}$$

where the term in angle brackets is the one-electron integral:

$$\langle i|\hat{h}|i\rangle = \int \chi_i^*(\boldsymbol{x_1})\hat{h}(i)\chi_j(\boldsymbol{x_1})d\boldsymbol{x_1} \tag{48}$$

and the term in square brackets is the two-electron integral:

$$[ij|kl] = \int \chi_i^*(\boldsymbol{x_1})\chi_j(\boldsymbol{x_1})\frac{1}{r_{ij}}\chi_k^*(\boldsymbol{x_2})\chi_l(\boldsymbol{x_2})d\boldsymbol{x_1}d\boldsymbol{x_2} \tag{49}$$

The HF method assumes that the wavefunction can be approximated by a single Slater determinant made up of one spin orbital per electron. Now the goal is to minimize the Hartree-Fock energy expression with respect to changes in the orbitals $\chi_i \rightarrow \chi_i + \delta\chi_i$. The spin-orbitals are assumed to be orthonormal ($\langle i|j\rangle = \delta_{ij}$) and the variational procedure should also leave them orthonormal. This can be accomplished by Lagrange's method of undetermined multipliers. The end result is the HF equation:

$$\left[\hat{h}(\boldsymbol{x_1}) + \sum_{j\neq i}^{n}\left[\mathcal{J}_j(\boldsymbol{x_1}) - \mathcal{K}_j(\boldsymbol{x_1})\right]\right]\chi_i(\boldsymbol{x_1}) = \epsilon_i\chi_i(\boldsymbol{x_1}) \tag{50}$$

from this equation we obtain the energy eigenvalues ϵ_i for the spin orbital i. The two new terms introduced are the Coulomb operator $\mathcal{J}_j$ and the exchange operator $\mathcal{K}_j$. The Coulomb operator gives the average local potential at point $\boldsymbol{x_1}$ due to the charge distribution at $\boldsymbol{x_2}$ from the electron in orbital j:

$$\mathcal{J}_j(\boldsymbol{x_1}) = \int \frac{|\chi_j(\boldsymbol{x_2})|^2}{r_{12}}d\boldsymbol{x_2} \tag{51}$$

The exchange operator does not have a a simple classical analog like the Coulomb operator and it is the result from the antisymmetry requirement of the wavefunction. It exchanges spin orbitals χ_i and χ_j, it can be defined by its action on an arbitrary spin orbital χ_i:

$$\mathcal{K}_j(\boldsymbol{x_1})\chi_i(\boldsymbol{x_1}) = \left[\int \frac{\chi_j^*(\boldsymbol{x_2})\chi_i(\boldsymbol{x_2})}{r_{12}}d\boldsymbol{x_2}\right]\chi_j(\boldsymbol{x_1}) \tag{52}$$

In equation 50 the action on the spin-orbital χ_i can be treated as a single *Fock operator*:

$$\hat{f}(\boldsymbol{x_1})\chi_i(\boldsymbol{x_1}) = \epsilon_i\chi_i(\boldsymbol{x_1}), \quad \hat{f}(\boldsymbol{x_1}) = \hat{h}(\boldsymbol{x_1}) + \sum_{j}^{n}\left[\mathcal{J}_j(\boldsymbol{x_1}) - \mathcal{K}_j(\boldsymbol{x_1})\right] \tag{53}$$

The solutions to these equations are found by guessing an initial trial orbital wavefunction, calculating the Fock operator. Solving the HF equation then results in a new orbital wavefunctions. Next, these new orbitals are used for further calculations and this process is repeated until reaching convergence. This iterative procedure is called a self-consistent-field (SCF) approach.

3.3.2 Restricted and Unrestricted Hartree-Fock

The HF method described above assumes that the spatial part of the spin orbital is the same for both spin up (α) and spin down (β) electrons. This assumption arises because only orbitals fully occupied by two electrons are allowed. This ensures that the interaction between electrons of the same spin is treated equally for both spin up and spin down electrons. This scenario, where orbitals are fully occupied, is referred to as the restricted Hartree-Fock (RHF) method.

In contrast, when dealing with a system composed of an unequal number of spin up and spin down electrons, the spatial part of their spin-orbitals must differ. This leads to a set of coupled equations, characteristic of the spin unrestricted Hartree-Fock (UHF) method.

3.3.3 Dirac-Hartree-Fock

The entire procedure discussed in the previous section was conducted within the non-relativistic framework. The one-electron operator includes only a kinetic term, without any added mass terms. If the HF procedure is conducted with relativistic effects taken into account, the free electron Dirac Hamiltonian is employed as the one-electron operator. In this scenario, the method is referred to as the Dirac-Hartree-Fock (DHF) method.

3.3.4 Electron Correlation Methods

The Hartree-Fock (HF) method generates solutions to the Schrödinger equation by replacing the actual electron-electron interaction with an average mean field interaction. In a large basis set, the HF wave function can account for approximately 99 percent of the total energy, but the remaining 1 percent is crucial for accurately describing chemical phenomena [40]. The energy difference between the HF solution and the lowest possible energy in the given basis set is known as the electron correlation (EC) energy. This EC energy arises from Coulomb correlation interactions and Fermi correlation interactions. The former correlates electrons with opposite spins, while the latter correlates electrons with the same spin. Coulomb correlation occurs more frequently, as it is present for electrons both in the same orbital and in different orbitals.

In HF methods, a single Slater determinant is used, where electrons in the same spin-orbital have a spatial overlap of one, but with opposite spins. For electrons in different spin-orbitals, the spatial overlap is zero [40]. Consequently, the HF method completely ignores Coulomb correlation because the wave function only accounts for interelectronic repulsion in an average manner [47]. This limitation can be addressed more effectively by using dynamic correlation methods, which consider electron excitations.

3.3.5 Coupled Cluster

Coupled cluster (CC) is one of the most commonly used methods among several post-Hartree–Fock *ab initio* quantum chemistry methods. The CC method effectively addresses the problem of electron correlation encountered in HF theories [47]. In this section, we follow the derivation by A.A. Hasanein and M.W. Evans in [47]. The CC method is based on an exponential operator:

$$\Psi = e^{\hat{T}}\Phi_0 \tag{54}$$

which is added to the Slater determinant Φ_0. The argument in the exponent, $\hat{T}$, is an operator that generates excitations from an independent particle model wave function Φ_0. This wave function, Φ_0, can represent either a closed shell (RHF) or open shell (UHF) single determinant composed of molecular spin-orbitals. The operator $\hat{T}$, known as the cluster operator, is expressed as follows:

$$\hat{T} = \hat{T}_1 + \hat{T}_2 + ... + \hat{T}_n \tag{55}$$

where $\hat{T}_1$ is the one-particle excitation operator and $\hat{T}_2$ is the two-particle excitation operator. The letter n stands for the number of electrons in the molecule. The action of the first two operators is given by:

$$\hat{T}_1\Phi_0 = \sum_{r,k} t_r^k D_r^k \quad ; \quad \hat{T}_2\Phi_0 = \sum_{\substack{r>s \\ k>l}} t_{rs}^{kl} D_{rs}^{kl} \tag{56}$$

where the letters p, q, r, s... stand for the occupied orbitals and the letters i,j,k,l,...stands for the unoccupied virtual orbitals. The terms t_{rs}^{kl}...etc, are the operator coefficients which give the amplitude of the transition. D_r^k is a singly excited determinant and D_{rs}^{kl} is a doubly excited determinant. The single excitation operator excites the electron from orbital r to the virtual orbital k as described by D. The equation for the rest of operators is similar to the the ones shown above, they are formed out of a linear combination of excited determinants. The maximum amount of excited electrons that can exist in the system is n so $\hat{T}_n$ is the last operator available.

The term in exponential form in equation 54 can expanded through Taylor expansion to get:

$$\exp\left\{\hat{T}\right\} = 1 + \hat{T} + \frac{\hat{T}^2}{2!} + \frac{\hat{T}^3}{3!} + ... \tag{57}$$

and equation 54 obtains the form:

$$\Psi = \left[1 + \hat{T} + \frac{\hat{T}^2}{2!} + \frac{\hat{T}^3}{3!} + ...\right]\Phi_0 \tag{58}$$

Now, equation 55 for the overall cluster operator is inserted in to equation 58 with the corresponding expression 56 for each operator of $\hat{T}$. Performing this operation would resemble the full CI calculation and it would give the exact wavefunction and correlation energy of the system [47]. Normally the full CI calculations are not carried out as they require a lot of computational cost. It is more common to truncate the expression for the cluster operator and only use the first couple of operators in equation 55. If only $\hat{T}_1$ and $\hat{T}_2$ are utilized, then it is called the CC singles and doubles (CCSD) method. When utilizing this method we use the following expression for the wavefunction:

$$\Psi = e^{\hat{T}}\Phi_0 = e^{(\hat{T}_1+\hat{T}_2)}\Phi_0 = \left[1 + \hat{T}_1 + \hat{T}_2 + \frac{(\hat{T}_1 + \hat{T}_2)^2}{2!}\right]\Phi_0 \tag{59}$$

where we get double excitation determinants originating both by a two-particle excitation operator $\hat{T}_2$ and by the product of two consecutive one-particle operator $\frac{1}{2!}\hat{T}_1^2$. Although they both will give double excitation orbitals, the amplitude for the latter case will be given by a product of two separate coefficients $t_r^k t_s^l$ instead of a single amplitude coefficient t_{rs}^{kl}. The terms consisting of both one and two-particle excitation operators $\frac{1}{2!}\hat{T}_1\hat{T}_2$ will resemble triple excitations. Ultimately, the square of the two-particle operator will address the case for quadruple excitations.

Although used extensively, the coupled cluster singles and doubles (CCSD) method is not sufficient when highly accurate results are required [48]. The CCSDT which includes the three-particle excitation operator $\hat{T}_3$ gives results in excellent agreement with those obtained with full CI, but the cost of CCSDT is high enough to severely restrict its application. A computationally cheaper approximation to CCSDT can be done by introducing a perturbative estimate of the connected triple excitations, this is done in methods such like CCSD(T) [49]. This method includes perturbations up to fifth order in the expansion of $\exp\left\{\hat{T}_1 + \hat{T}_3 + \hat{T}_3\right\}$. Other methods only introduce new perturbations up to fourth order like the CCSD+T [49]. All these CC methods guarantee size extensivity[9] and size consistency[10] but they are not variational like HF. [50].

3.3.6 Møller-Plesset Perturbation Theory

Møller-Plesset (MP) perturbation theory is another of the theories addressing the problem of electron correlation faced in HF methods. It is a perturbation method like CC but this time a perturbation is applied on the Hamiltonian.

[9] Means that the energy should grow linearly with the number of electrons in the system.

[10] Property that guarantees the consistency of the energy behaviour when the interaction between the involved molecular system is nullified.

The basic idea behind perturbation theory is that if the description of a simple system is known, then a more complex version of this system can be treated mathematically as an altered (perturbed) version of the simple one [51]. This section is based on the derivation of C.J.Cramer [52]. In perturbation theory, the overall Hamiltonian is described as:

$$\hat{H} = \hat{H}^{(0)} + \lambda V \tag{60}$$

where we have an unperturbed Hamiltonian with a perturbing term V parameterized by λ. In MP he unperturbed Hamiltonian is taken as the sum of one-electron Fock operators:

$$\hat{H}^{(0)} = \sum_{i=1}^{n} \hat{f}_i \tag{61}$$

where n is the number of basis functions. The zeroth-order eigenvalue for the unperturbed Hamiltonian is given then by:

$$\hat{H}^{(0)}\Psi^{(0)} = \sum_{i}^{occ} \epsilon_i \Psi^{(0)} \tag{62}$$

where we are summing over the occupied orbitals and $\Psi^{(0)}$ is the HF wavefuntion. The perturbation term V is given in the following expression as:

$$V = \sum_{i}^{occ}\sum_{i>j}^{occ} \frac{1}{r_{ij}} - \sum_{i}^{occ}\sum_{j}^{occ}\left(\mathcal{J}_{ij} - \frac{1}{2}\mathcal{K}_{ij}\right) \tag{63}$$

where we are summing over MO orbitals instead of AO orbitals. Now we can compute the first-order correction to the zeroth-order energy by finding the expectation value, which will give the HF energy:

$$E^{(0)} + E^{(1)} = \langle\Psi^{(0)}|\hat{H}^{(0)}|\Psi^{(0)}\rangle + \langle\Psi^{(0)}|V|\Psi^{(0)}\rangle = E_{HF} \tag{64}$$

If only the first-order correction is applied to the energy then the method is known as MP1. No electron correlation has been added until now. In order to account for it, it is necessary to compute the second order energy correction also which is given by:

$$E^{(2)} = \sum_{j>0} \frac{|\langle\Psi_j^{(0)}|V|\Psi_0^{(0)}\rangle|^2}{E_0^{(0)} - E_j^{(0)}} \tag{65}$$

If this expression for the second-order correction is furthered derived using the Condon–Slater rules and Brillouin's theorem[11], then the final form for $E^{(2)}$ is:

$$E^{(2)} = \sum_{i}^{occ}\sum_{j>i}^{occ}\sum_{a}^{vir}\sum_{b>a}^{vir} \frac{[(ij|ab) - (ia|jb)]^2}{\epsilon_i + \epsilon_j - \epsilon_a - \epsilon_b} \tag{66}$$

where in this case the indices a and b stand for virtual orbitals. Combining all this corrections in a sum we obtain the MP2 method. Additional energy correction can be added to the total energy, if enerfy corrections up to n-order are counted then the method is termed MPn. In the case of MP2 the final energy would be:

$$E_{MP2} = E^{(0)} + E^{(1)} + E^{(2)} \tag{67}$$

MP2 methods do not take a lot of computaational time and can be efficiently evaluated. They scale with N^5 where N is the number of basis functions.

[11] Integrals involving the singly excited determinants will all be zero [52].

4 Results

In the following section, we present the results obtained from this study. The first part focuses on the results obtained for the SrF molecule, exploring how various computational parameters such as basis sets, computational method, virtual space and electron correlation influence the value of W_{PV}. The second part of the results discusses the calculations performed for the other molecules under investigation (YF+, CF, NF+, XeF, XeF2) where it is examined how this molecules can exhibit distinct W_{PV} values.

4.1 Molecular Geometries

Before performing any calculations on W_{PV}, it is crucial to accurately establish the geometry of the molecules under study. This process began by searching the literature for experimental geometries of the molecules in question. For most molecules, experimental geometries were readily available and served as a reliable basis for subsequent calculations.

In cases where experimental geometries were not found in the literature, a geometry optimization was carried out using the CCSD(T) method. This was necessary for molecules such as XeF and YF+, where experimental geometries were absent. Geometry optimization ensures that the molecular structure used in W_{PV} calculations is as accurate as possible, even in the absence of experimental data.

For the geometry optimizations, an initial guess for the geometry is required. The initial geometry for XeF was specified with a bond length of 1.979 Å, equal to that found in the bond of XeF2 between the Xe and F atoms [53]. For YF+ the initial bond length was found in the literature with a value of 1.883 Å. This value was obtained through computational methods, using the equation-of-motion coupled cluster method (EOM-CC) [54].

Both geometry optimizations were performed using the dyall.v4z basis set and included full electron correlation. A virtual space cutoff of 100 a.u and a 4-component Hamiltonian were employed. Table 1 shows all the final molecular geometries employed for the molecules in this work.

Table 1: Geometries of diatomic molecules, bond lengths are given in Angstrom, 1Å= 1×10^{-10}m [55].

Molecule	**Bond Length r_e, [Å]**	**Reference**	**Method**
XeF	2.10558	This work	CCSD(T)
YF+	1.88737	This work	CCSD(T)
SrF	2.075	[56]	Experiment
CF	1.267	[57]	Experiment
NF+	1.180	[58]	Experiment

4.2 Calculations for the Enhancement Factor W_{PV} in SrF

In this section of the paper, we present the results obtained for the enhancement factor W_{PV} of both atoms in SrF. The first results can be seen in Table 2.

Table 2: Calculated W_{PV} coefficients (Hz) for both Sr and F. Calculations were done with all electrons correlated and a virtual space cut-off of 500 a.u. was used together with dyall.v4z basis sets.

Method	W_{PV} (Hz), Sr	W_{PV} (Hz), F
CCSD(T)	63.2156	0.23393

These initial results show that the metal atom Sr has an enhancement factor W_{PV} several times higher than the lighter atom F. This means that the atom Sr is more sensitive to the NSD-PV effect, and as shown in other works [15] it follows the pattern of the metal atom being the most sensitive to this effects.

Calculations of W_{PV} were conducted separately for both atoms in the molecule. The results were obtained using the DHF, MP2, CCSD, and CCSD methods with various treatments of triple excitations (CCSD(T), CCSD-T, CCSD+T). Although triple excitations are included to varying extents, most results will be presented for the CCSD(T) method only, as it is the most commonly used.

4.2.1 Basis Set Quality

As it was previously mentioned, the computational parameters involved in the calculation of SrF were varied in order to assess its effect on the final value of W_{PV}.The first parameter studied was the size of the basis set. The cardinality of the basis sets was varied, utilizing double-, triple-, and quadruple-zeta basis sets. Specifically, the standard Dyall's relativistic basis sets were employed. Additionally, diffuse functions were added to the dyall.v4z basis set to examine their influence on the calculations. The dyall.v4z basis set was augmented using the s-aug-dyall.v4z, which adds a single diffuse function for each symmetry, and the d-aug-dyall.v4z, which adds two diffuse functions for each symmetry. The addition of diffuse fucntions will help improve the description of the atomic orbitals in the outer regions of the molecule. However, parity-violating effects primarily arise from nuclear processes, so an accurate description of the electronic orbitals near the nucleus is crucial to obtain reliable results. Furthermore, it has been shown in previous works that the addition of tight s and p functions alter significantly the value of the W_{PV} parameter [4, 13, 17]. Consequently, the effects of adding tight functions to the basis sets were also studied. The addition of tight and diffuse function was done separately for each atom in the molecule. All calculations were done with 37 correlated electrons, an electron correlation of 0.79[12] (corresponding to a cut-off energy of -30.0 a.u. in the occupied orbitals). The virtual space energy cut-off was set at +30.0 a.u., all orbitals above this energy were excluded. In Table 3 the results for W_{PV} of F in SrF are shown.

Table 3: Basis set dependence of the W_{PV} (Hz) coefficient for the F atom in SrF. Calculations were carried with an occupied and virtual space cut-off of $\pm$30 a.u.

Basis Set Size					
Basis (Sr)	Basis (F)	DHF	MP2	CCSD	CCSD(T)
dyall.v2z	dyall.v2z	0.08022	0.11435	0.21877	0.22491
dyall.v3z	dyall.v3z	0.08654	0.12296	0.21077	0.21727
dyall.v4z	dyall.v4z	0.09038	0.12698	0.21701	0.22211
Diffuse Functions					
Basis (Sr)	Basis (F)	DHF	MP2	CCSD	CCSD(T)
s-aug-v4z	dyall.v4z	0.09008	0.12892	0.21652	0.22230
d-aug-v4z	dyall.v4z	0.09008	0.12809	0.21569	0.22230
dyall.v4z	s-aug-v4z	0.09008	0.12809	0.21569	0.22313
dyall.v4z	d-aug-v4z	0.08925	0.12809	0.21652	0.22230
Tight Functions					
Basis (Sr)	Basis (F)	DHF	MP2	CCSD	CCSD(T)
dyall.v4z	dyall.v4z + ts	0.09057	0.12892	0.21718	0.22362
dyall.v4z	dyall.v4z + tp	0.09289	0.13198	0.22230	0.22891
dyall.v4z	dyall.v4z + ts + tp	0.09313	0.13239	0.22280	0.22941

With regards to the size of the basis set used, when moving from double to triple-zeta basis set the W_{PV} value increases by $\sim 7.88\%$ for DHF and by $\sim 7.53\%$ for MP2. On the contrary, for CCSD and CCSD(T), when going from double to triple-zeta basis the W_{PV} value decreases. For CCSD the value decrease by $\sim 3.66\%$ and for CCSD(T) by $\sim 3.40\%$. As expected, both the CCSD and CCSD(T) methods scale similarly, while the DHF and MP2 methods also exhibit similar scaling behavior when increasing the basis set. Upon further increasing the

[12] Electron correlation is given by $\frac{N_{correlated}}{N_{total}}$.

basis set size from triple-zeta to quadruple-zeta, we again observe an increase in W_{PV} for both DHF ($\sim 4.44\%$) and MP2 ($\sim 3.27\%$). In the case of both CCSD methods the W_{PV} value also increases ($\sim 2.96\%$ for CCSD and $\sim 2.23\%$ for CCSD(T)), unlike in the previous situation; however, going from double to quadruple-zeta still decreases the W_{PV} value. In Figure 3 we can see these results in plot form, with two plots showing the overall behaviour of the different methods with increasing basis set size. We can see that MP2 and DHF show a similar scaling and pattern, while CC methods exhibit a completely different behavior compared to both of these.

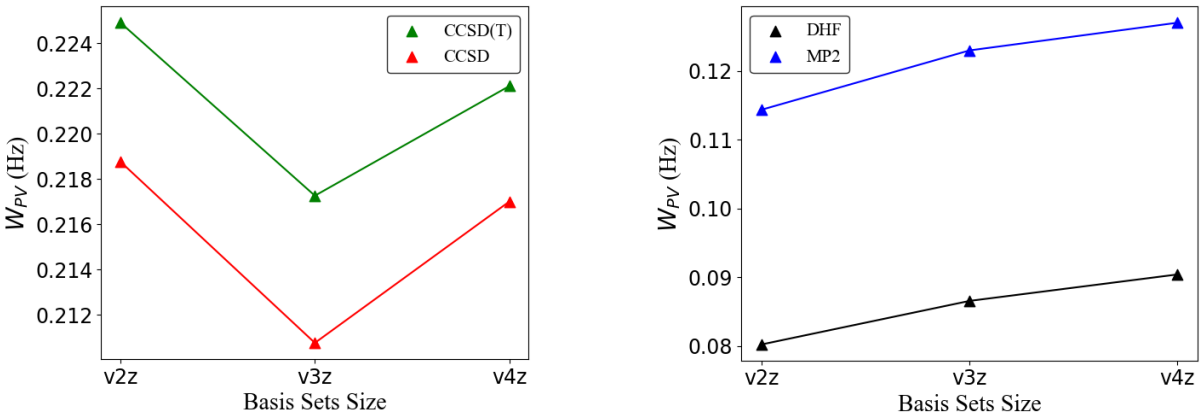

(a) Results at the CCSD level.

(b) Results at the DHF and MP2 level

Figure 3: Calculated W_{PV} coefficient of F in SrF for increasing basis set size.

Initially, upon examining the data, it appears that the addition of diffuse functions has minimal impact on the final value of W_{PV}. As mentioned earlier, diffuse functions are applied individually to each atom within the molecule. At the DHF level, only the introduction of the diffuse function (d-aug-v4z) to the fluorine atom shows any notable effect on W_{PV}, resulting in a decrease of approximately $\sim 1.25\%$. Conversely, for MP2 calculations, the inclusion of diffuse functions (s-aug-v4z) to the strontium atom has a discernible influence on W_{PV}, leading to an increase of about $\sim 1.53\%$. However, at both the CCSD and CCSD(T) levels, the incorporation of diffuse functions does not yield significant changes, with all variations remaining below one percent.

With respect to the addition of tight functions, the augmentation with s functions increases the W_{PV}, although the increase is minimal. At the CCSD level, the changes in W_{PV} are approximately $\sim 0.08\%$, indicating a negligible effect. For DHF and CCSD(T), the changes are more substantial, with increments of $\sim 0.21\%$ and $\sim 0.68\%$, respectively. However, the response to tight s functions does not seem to be significant overall. It is also notable how CCSD and CCSD(T) diverge significantly in their responses. The highest response to the addition of tight s functions is observed at the MP2 level, with an increment of $\sim 1.53\%$.

The effect of p functions is considerably larger, resulting in a more substantial increase in W_{PV}. At the DHF level, the increase is approximately $\sim 2.78\%$, while for CCSD, it is $\sim 2.44\%$. For CCSD(T), the increase is $\sim 3.06\%$, and for MP2, it is $\sim 3.94\%$. The last line of Table 3 presents the results for calculations that combine both tight s and p functions.

Basis sets were also varied for the heavy atom and the results for W_{PV} of Sr are shown in Table 4.

In the case for W_{PV} of Sr, when going from double to triple-zeta basis set there is an increase in W_{PV} for all methods unlike for F. For DHF and MP2, the W_{PV} value increases by $\sim 11\%$ whereas for CCSD and CCSD(T) the increase is by $\sim 9.4\%$. When going from triple to quadruple-zeta basis sets there is a further increase in W_{PV} of $\sim 4.9\%$ for both DHF and MP2 and of $\sim 4.6\%$ for CCSD and CCSD(T). Although all methods scale similarly, it is observed that the increase for both CCSD methods is slightly lower compared to DHF and MP2. In Figure 4 results are shown again in plot form, showing the behaviour of all the methods with respect to the basis set size.

In the case of Sr, all computational methods demonstrate a consistent scaling pattern. This contrasts sharply with the behavior observed for F, where CC methods diverge significantly from both DHF and MP2 methods.

Table 4: Basis set dependence of the W_{PV} (Hz) coefficient for the Sr atom in SrF. Calculations were carried with an occupied and virtual space cut-off of ± 30 a.u.

Basis Set Size					
Basis (Sr)	Basis (F)	DHF	MP2	CCSD	CCSD(T)
dyall.v2z	dyall.v2z	39.7534	47.6909	53.9326	53.4262
dyall.v3z	dyall.v3z	44.2184	52.8391	59.0204	58.4537
dyall.v4z	dyall.v4z	46.3328	55.5074	61.7712	61.1573
Diffuse Functions					
Basis (Sr)	Basis (F)	DHF	MP2	CCSD	CCSD(T)
s-aug-v4z	dyall.v4z	46.3245	55.5074	61.7558	61.1401
d-aug-v4z	dyall.v4z	46.3468	55.5470	61.7764	61.1855
dyall.v4z	s-aug-v4z	46.2980	55.4743	61.6202	60.9971
dyall.v4z	d-aug-v4z	46.2831	55.2917	61.5847	60.9294

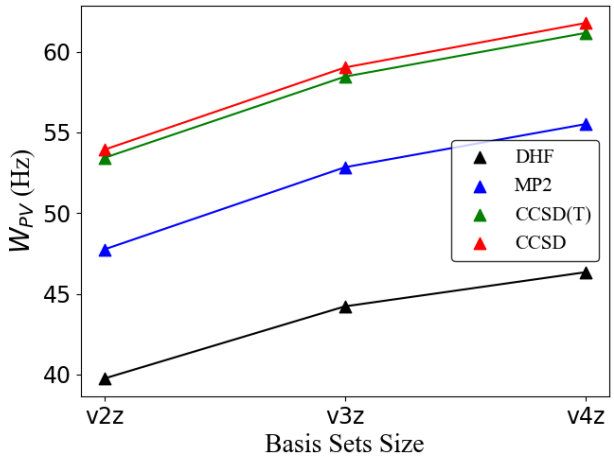

Figure 4: Calculated W_{PV} coefficients of Sr in SrF for increasing basis set size.

Looking at the addition of diffuse functions in the case for W_{PV} of Sr, once again it seems to have no significant impact on W_{PV}. Augmenting the basis set of Sr with diffuse functions has virtually zero impact on the final value of W_{PV} ($\sim 0.03\%$). Conversely, augmenting the basis set of F alters the W_{PV} value more noticeably. The addition of two diffuse functions for each symmetry (d-aug-v4z) for the fluorine atom decreases the value of W_{PV} by approximately 0.11% for DHF and by about 0.35% for methods incorporating electron correlation treatment.

4.2.2 Electron Correlation and Virtual Space Cut-off

This section explores how the number of correlated electrons and the size of the virtual energy space affect W_{PV}. Initially, the influence of the number of correlated electrons on the value of W_{PV} for both fluorine and strontium atoms will be examined, as electron correlation can significantly impact the computed properties and overall accuracy of the results.

Subsequently, the focus will shift to the virtual energy space, a critical factor in determining the precision and reliability of quantum chemical calculations. By investigating these variables, we aim to identify the optimal computational settings needed to achieve the most accurate and reliable results. Both sets of calculations were performed using dyall.v4z basis sets for both atoms, chosen for their high accuracy in representing the electronic structure.

In this initial set of calculations, the number of correlated electrons is varied from 17 electrons (~ -5 a.u. cut-off in the occupied orbital space) up to a 47 electrons (~ -600 a.u. cut-off in the occupied orbital space) which is the total number of electrons present in SrF. The virtual energy cut-off was set at a high value of 500 a.u., ensuring that a substantial portion of the virtual space is included in the analysis. This comprehensive approach allows for a detailed examination of how electron correlation influences W_{PV}.

In Figure 5 the trend for W_{PV} of F with respect to the number of correlated electrons is shown at the MP2, CCSD and CCSD(T) level. MP2 and CCSD methods are shown in separate graphs in order to give a better depiction of the results.

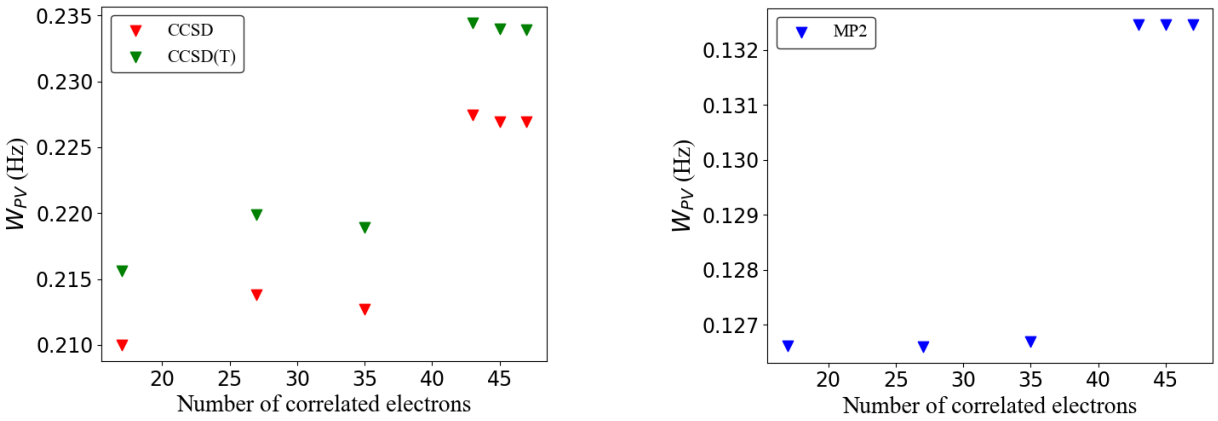

(a) Results at the CCSD level.

(b) Results at the MP2 level

Figure 5: Calculated W_{PV} coefficient of F in SrF for different numbers of correrlated electrons.

In Figure 5, we observe that the number of correlated electrons has a significant impact on the W_{PV} value. Increasing the number of correlated electrons from 17 to 47 results in an approximate W_{PV} increase of $\sim 4.63\%$ for MP2. The effect is even more pronounced for CC methods, with increments of around $\sim 8.07\%$ for CCSD and $\sim 8.49\%$ for CCSD(T). Notably, the primary contributor to this increase in W_{PV} for both CC and MP2 methods occurs when we go from 35 correlated electrons to 43 correlated electrons. This specific step accounts for an increment in W_{PV} of $\sim 4.57\%$ for MP2 (99% of the total increase) and $\sim 6.76\%$ and $\sim 6.94\%$ for CCSD and CCSD(T), respectively (around 83% of the total increase). Beyond this step, W_{PV} does not appear to undergo any more significant changes.

Now, the focus shifts towards examining the effects that the number of correlated electrons has on the W_{PV} value of the Sr atom. The computational parameters were kept consistent throughout the analysis to ensure comparability of the results. Figure 6 presents the results, showing how varying the number of correlated electrons impacts the W_{PV} value of Sr.

It is evident that the number of correlated electrons has a substantial impact on the final W_{PV} value. Increasing the number of correlated electrons from 17 to 47 results in an increase in W_{PV} of approximately $\sim 5.96\%$ at the MP2 level and $\sim 8.6\%$ at both the CCSD and CCSD(T) levels. Notably, the increase in W_{PV} with an increasing number of correlated electrons is more gradual compared to the previous case for the F atom, although several key features warrant attention. The average increase in W_{PV} per step increase in correlated electrons is $\sim 1.18\%$ for MP2 and $\sim 1.68\%$ for the CC methods. However, examining the W_{PV} increments at each individual step reveals that the transition from 27 to 35 correlated electrons results in an increment of $\sim 4.09\%$ for MP2 (69% of the total increase) and $\sim 4.96\%$ for the CC methods (58% of the total increase), approximately three times greater than the average W_{PV} increment per step. Similar to the case with the F atom, although to a lesser extent, there is a specific range of electrons in the occupied orbital energy space (from 27 to 35 for Sr and from 35 to 43 for F) that primarily contributes to the overall increase in W_{PV}.

Now our attention goes towards the impact the virtual space energy cut-off has on the calculations. This set of calculations were done once again with dyall.v4z basis sets for both atoms and with all electrons correlated. The

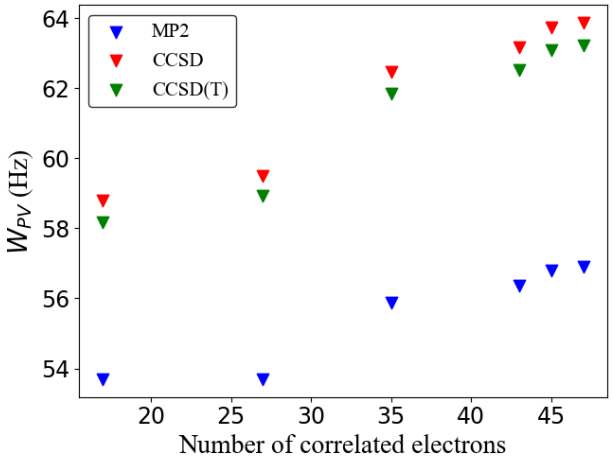

Figure 6: Calculated W_{PV} coefficients of Sr in SrF for different numbers of correlated electrons.

virtual space energy cut-off was varied extensively, starting from 10 a.u. and increasing incrementally up to a substantial value of 1000 a.u., to thoroughly investigate the impact on the computational results. In Figure 7 the results for the F atom are shown, MP2 and CC methods are once again given in separate plots.

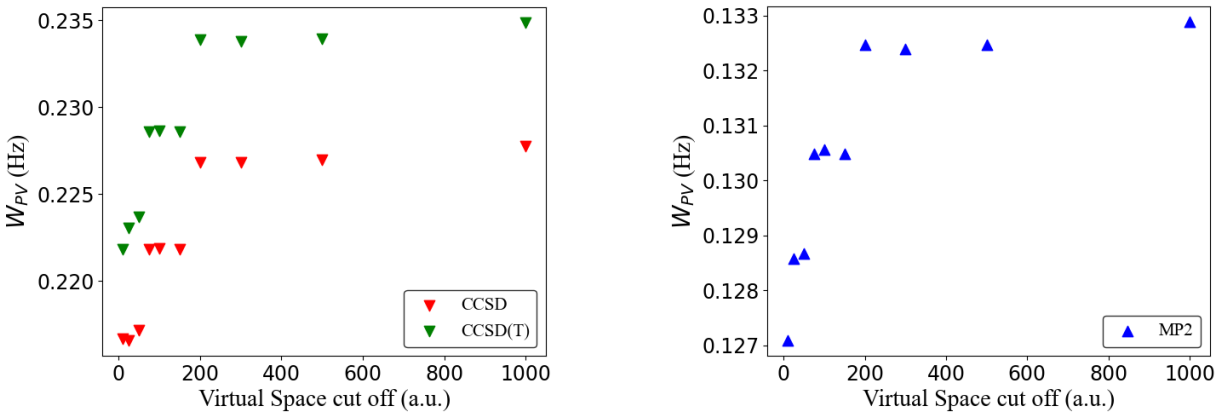

(a) Results at the CCSD level.

(b) Results at the MP2 level

Figure 7: Calculated W_{PV} coefficient of F in SrF for different sizes of the virtual energy space.

Yet again, like for the electron correlation, it is evident that the size of the virtual space has a important effect on the calculation. Augmenting the size of the virtual space from 10 a.u. up to 1000 a.u. increase the W_{PV} value by $\sim 4.55\%$ for MP2 and by $\sim 5.11\%$ and $\sim 5.89\%$ for CCSD and CCSD(T) respectively. The W_{PV} value increases considerably for both MP2 and CC methods until reaching the virtual space cut-off of 200 a.u., after this point the W_{PV} keeps increasing but with a much lower rate. Going from 10 a.u. to 200 a.u. accounts for $\sim 93\%$ of the total W_{PV} increase while the remaining $\sim 7\%$ comes from going from 200 a.u. to 1000 a.u., this occurs for all the methods employed.

A more detailed analysis of the plots in Figure 7 reveals that this overall W_{PV} increment, occurring from 10 a.u. to 200 a.u., does not manifest gradually but rather in jumps instead. As the virtual space increases, we can observe that the W_{PV} values cluster into three groups for CCSD and CCSD(T), and into four groups for MP2.

For CCSD, the change in W_{PV} is approximately $\sim 0.23\%$ when the virtual space energy cutoff is increased from 10 a.u. to 50 a.u. In contrast, the change in W_{PV} jumps to $\sim 2.13\%$ when the cutoff is extended from 50 a.u. to 75 a.u., a magnitude approximately ten times larger. This pattern repeats when transitioning from 75 a.u. to 150 a.u.,

where there is virtually no change ($\sim 0.0\%$), followed by another significant increase of $\sim 2.27\%$ when extending from 150 a.u. to 200 a.u.

At the CCSD(T) level, the plot exhibits a nearly identical pattern to CCSD, with changes occurring at the same intervals and with increments of approximately $\sim 2.18\%$ and $\sim 2.31\%$, respectively. However, upon closer comparison of the initial clusters in CCSD and CCSD(T), the ones corresponding to the lowest values of W_{PV}, it is evident that the values are more dispersed in CCSD(T).

For MP2, unlike in the CC methods, the data values are grouped into four clusters instead of three. The cluster corresponding to the lowest W_{PV} values in the CC methods appears to split into two for the MP2 method. Significant increments in W_{PV} occur when transitioning from 75 a.u. to 150 a.u. and from 150 a.u. to 200 a.u., similar to the CC methods. Additionally, there is an additional increase in W_{PV} observed when moving from 10 a.u. to 25 a.u., attributed to the splitting in the initial cluster. The average increase in W_{PV} per transition is approximately $\sim 1.41\%$, which is lower compared to the CC methods ($\sim 2.23\%$ per transition).

The size of the virtual space was varied as well in calculations for the W_{PV} value of Sr in SrF. Computational parameters and virtual space values were kept the same. Figure 8 shows the results obtained.

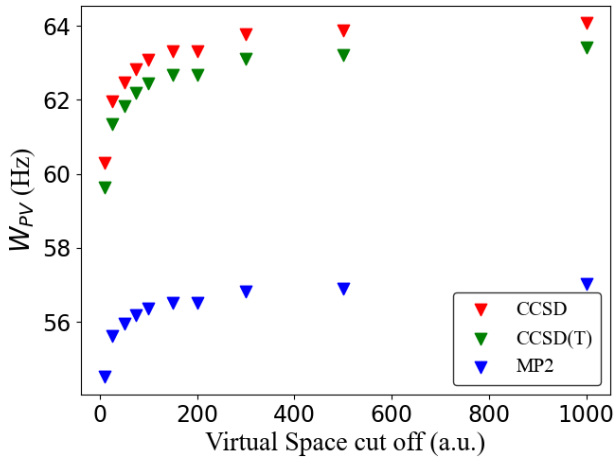

Figure 8: Calculated W_{PV} coefficient of Sr in SrF for different sizes of the virtual energy space.

The size of the virtual space has once again a significant impact on the final value of W_{PV}. The increment when going from 10 a.u. to 1000 a.u. is in this case of $\sim 4.62\%$ for MP2 and of $\sim 6.3\%$ for the CC methods. We see again a decay in the rate of change of W_{PV} with respect to the size of the virtual space, this can be seen as the W_{PV} value barely changes for virtual space energy cut-offs above 500 a.u.. However, in contrast with the previous case for the F atom, the increment in W_{PV} follows a more gradual pattern and no clusters of values are formed.

4.2.3 Computational Method

When examining the results for W_{PV} of F, the first notable observation is the dramatic change in W_{PV} with different computational methods. In Table 3 it is shown how methods incorporating electron correlation yield significantly higher values compared to the DHF method, which does not account for electron correlation. To emphasize the importance of electron correlation, transitioning from DHF to CCSD methods results in a W_{PV} value increase of approximately $\sim 152\%$, more than 2.5 times larger than without electron correlation.

Electron correlation at the MP2 level also notably affects the W_{PV} value, leading to an increase of approximately $\sim 42\%$ compared to the DHF value. Despite this significant increase, the MP2 method still underestimates the W_{PV} value, differing by 70% compared to the CCSD method.

Electron correlation also plays a crucial role in calculations for Sr. The results shown in Table 4 indicate that going from DHF to CCSD increases the W_{PV} value by $\sim 33\%$ where as going from DHF to MP2 causes an increment of $\sim 19.2\%$. Unlike for the F atom, MP2 performs substantially better in this case, capturing most of the electron

correlation and differing from CCSD only by $\sim 11\%$. These results highlight that while electron correlation is important for Sr calculations, its significance is not as pronounced as it is for F.

Incorporating triple excitations is crucial as they significantly influence the final calculation results. To thoroughly investigate their impact, calculations were performed with varying degrees of triple excitation inclusion, employing methods such as CCSD(T), CCSD-T, and CCSD+T. As it was mentioned in the method section, CCSD+T only includes triple excitation up to fourth order, where as CCSD(T) includes up to fourth order plus an additional subset of fifth order terms. At last, CCSD-T adds an additional fifth order term to CCSD(T) [49].

Table 5: Calculated W_{PV} coefficients (Hz) for both Sr and F with different levels of triple excitations.

Method	W_{PV} (Hz), Sr	W_{PV} (Hz), F
CCSD	63.8668	0.22695
CCSD(T)	63.2156	0.23393
CCSD-T	63.2621	0.23259
CCSD+T	63.4981	0.24272

Table 5 shows the results for both Sr and F atoms, calculations were done with all electrons correlated, a virtual space cut-off of 500 a.u. was used together with dyall.v4z basis sets. In Figure 9 we can see the result shown in a plot for both F and Sr.

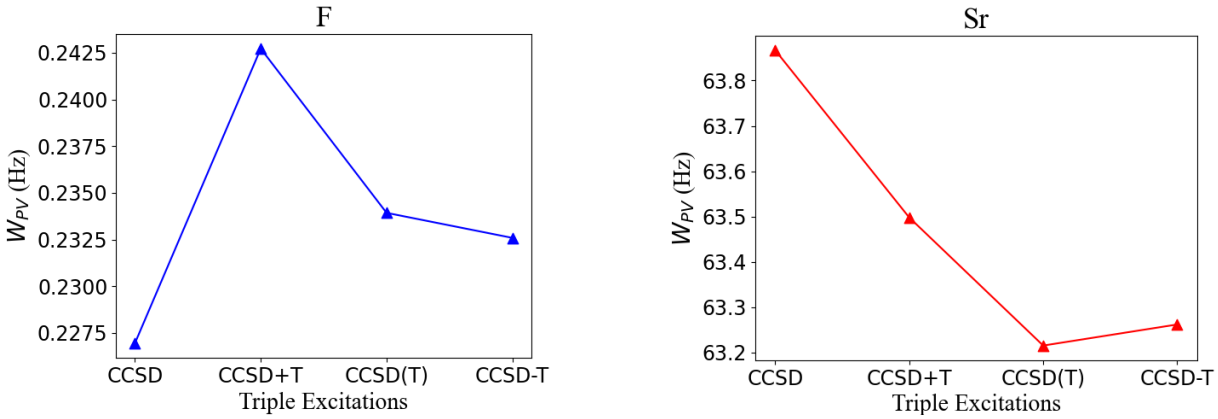

(a) W_{PV} of F.

(b) W_{PV} of Sr.

Figure 9: Calculated W_{PV} coefficients of both Sr and F in SrF for different degrees of triple excitations.

We first examine the impact of triple excitations on Sr. Incorporating triple excitations up to the fourth order in the CCSD calculations results in a decrease of W_{PV} by approximately $\sim 0.58\%$. Further addition of triple excitations at the fifth order results in an additional decrease in W_{PV} by $\sim 0.44\%$. The inclusion of an extra term at the fifth order slightly moderates the contribution of triple excitations, but this effect is minimal ($\sim 0.07\%$). As an overall effect, it seems like the addition of triple excitations lowers the W_{PV} value.

We now turn our attention to the F atom. The initial inclusion of triple excitations leads to a significant increase in W_{PV} by approximately $\sim 6.95\%$. However, incorporating further triple excitations at the fifth order has the opposite effect, resulting in a decrease of W_{PV} by $\sim 3.62\%$. Adding an extra term at the fifth order further reduces W_{PV} by $\sim 0.57\%$.

A notable observation from the results in Figure 9 is the contrasting effect of triple excitations on Sr and F. Generally, incorporating triple excitations increases the W_{PV} value for F, whereas it decreases the W_{PV} value for Sr. Additionally, the inclusion of fifth-order terms in Sr further accentuates the difference with respect to CCSD, whereas for F, it moderates the overall contribution of triple excitations. It is also worth mentioning that the impact of triple excitations is significantly greater for F than for Sr, as evidenced by the percentage differences. An

example of this is the negligible difference between CCSD(T) and CCSD-T for Sr, whereas for F, this difference is significant and should be taken into account.

4.3 Calculation of the Enhancement Factor W_{PV} for Fluorine in Various Molecular Systems

In this part of the result section we go over different types molecular system in order to examine how the W_{PV} of fluorine is affected by the molecular enviroment. The molecules under study are the following: YF+, CF, NF+, XeF.

As mentioned in the introduction, YF+ is isoelectronic with SrF, but its Y nucleus makes it a positive ion. Similarly, CF and NF+ share the isoelectronic characteristic with YF+ and SrF; however, CF and NF+ are lighter molecules with different open shell configurations. Finally, XeF has a heavier nucleus than SrF, making it interesting to investigate the implications this has on the W_{PV} value of F. Calculations where done with all electrons correlated for CF, NF+ and XeF molecules and with a virtual space cut-off of 200 a.u.. For YF+ calculations where done with an active space of ± 30 a.u.. Results of SrF with the same active space are given aswell, so they can be compared with YF+. All calculations were done with dyall.v4z basis sets and in Table 6 the results are shown for all the methods employed.

Table 6: Calculated W_{PV} coefficients (Hz) of F for different types of diatomic molecules.

Molecule	**DHF**	**CCSD**	**CCSD(T)**	**MP2**
Sr	0.09038	0.21701	0.22211	0.12698
YF+	0.00215	-0.09289	-0.08785	0.02239
CF	0.00232	0.00108	0.00145	0.00248
NF+	0.00718	0.00491	0.00589	0.00604
XeF	5,8246	6,8240	6,7012	6,2801

When looking at Table 6, we observe that in the first isolectronic pair (SrF, YF+) the molecules have contrasting results, with the enhancment factor W_{PV} of F being much lower in YF+ than in SrF. The biggest difference occurs at the DHF level with the W_{PV} value of F in SrF being around 40 times larger than in YF+. With the addition of electron correlation this difference lowers considerably, at the MP2 level the W_{PV} value of F in SrF is five times larger and in CC methods only two times larger.

For the second isoelectronic pair with lighter elements (CF, NF+), in contrast to SrF and YF+, this time is the positive ion the one that has the highest W_{PV} value. The W_{PV} value of F in CF is around 5 times smaller than in NF+ for CC methods. For DHF and MP2 the W_{PV} value is more or less 3 times smaller. Also for this lighter pair of isoelectronic systems, the difference in the DHF values is considerably to the one found for the heavier pair.

5 Discussion

In this discussion the first two sections critically interpret the computed W_{PV} values for fluorine (F) and strontium (Sr), focusing on the various computational parameters that have been tested. This analysis aims to provide insights into the factors shaping W_{PV} and their implications in molecular systems. Then, in the last section, the results obtained for the other molecules will also be interpreted in more detail.

5.1 SrF and Computational Parameters

Initial results of SrF showed that the metal atom Sr has an enhancement factor W_{PV} several times higher than the lighter atom F and this entails that the atom Sr is more sensitive to the NSD-PV effect. This could be explain due to the higher atomic number found in the metal atom in comparison to the fluorine atom. As it was discussed in the theory section, two of the NSD-PV sources present in the NSD-PV Hamiltonian 8 scale with the atomic number (κ_A and κ_{hfs}).

The impact of different computational parameters was studied for both atoms in the diatomic molecule SrF. A difference in behaviour was found between both atoms for many of the computational parameters present in the calculations.

The first aspect in which both atoms exhibit significant differences is related to the type of method employed in the calculations. The treatment of electron correlation is vital for both atoms; however, as highlighted in the results section, it is particularly critical for the lighter atom, fluorine (F). This is evidenced by the significant discrepancy between the DHF and CCSD results.

It is not only the inclusion of electron correlation that plays a crucial role but also the manner in which this electron correlation is implemented. This was observed in the results section, where discrepancies between MP2 and CCSD methods are several times greater for the F atom compared to the Sr atom.This same pattern was also observed when including triple excitations in CCSD, where the shift in W_{PV} for F was around ten times larger than that for Sr. These observations, derived from comparing Sr and F, underscore the critical importance of meticulously selecting computational methods for lighter systems. Such choices significantly influence the accuracy of result obtained.

Another notable difference between these atoms was observed in the size of their active spaces and its consequential impact on the final results. Transitioning from a low number of correlated electrons to all electrons being correlated had a similar impact on both atoms. However, as depicted in Figure 5 and Figure 6, the scaling of the enhancement factor with the number of correlated electrons differed between the two elements. Sr exhibited a gradual increase in the enhancement factor from 17 to 47 correlated electrons. In contrast, the behavior of fluorine (F) was distinct; it showed negligible change from 17 to 35 correlated electrons, with a noticeable alteration only occurring between 35 and 43 correlated electrons.

In SrF, the orbitals occupied between the 35th and the 43rd electrons include the 1s orbital of fluorine (F) and the 2p orbital of strontium (Sr). Notably, the 1s orbital of fluorine is higher in energy compared to the 2p orbitals of strontium. With this in mind, additional calculations were performed by including only the 1s orbital and excluding the 2p orbitals, resulting in a system with 37 correlated electrons. The difference in W_{PV} when transitioning from 37 to 43 electrons was approximately 0.003%, which is negligible. This demonstrates that the primary factor causing the sharp variation in W_{PV} for fluorine when adjusting electron correlation stems from the inclusion of the 1s orbital of fluorine (~ -26 a.u.). Therefore, incorporating all core orbitals of fluorine into the active space is crucial for accurately calculating the enhancement factor W_{PV} of fluorine.

Another aspect of the active space, the energy cutoff in the virtual space, also equally influences the final results of W_{PV} for both atoms. However, like for the number correlated electrons, the behaviour with increasing virtual energy cut-off was different again for each atom. The stronimum atom (Sr) showed a gradual change in the enhancement factor, reaching saturation at arounf 500 a.u.. Furthermore, the plot in Figure 8 exhibits a similar trend to that observed for the Ba atom in BaF when expanding the virtual space, as depicted in [4].

In contrast to Sr, the fluorine atom did not exhibit a gradual increase in the enhancement factor. As discussed in

the results section and illustrated in Figure 7, the increase in W_{PV} when expanding the virtual space occurs in two distinct jumps for CC methods and three jumps for MP2 methods.

5.2 Uncertainty

The study of the different computational parameters was used to determine the uncertainty in the final result of the W_{PV} value of F and Sr in SrF. The overall uncertainty is obtained by assesing the uncertainty arising in each of the computational parameter studied. All this different uncertainties are then combined to give the final total uncertainty. The combination of all these uncertainties is done assuming that they are independent from one another.

The first uncertainty comes from the choice of basis set. Uncertainty coming from basis set size was computed buy taking half the difference between the v4z and the v3z W_{PV} values. The uncertainty arising from diffuse functions was determined by calculating the difference between values obtained with and without diffuse functions. This same procedure was then used to obtained the uncertainty coming from tight functions in F. The difference between dyall.v4z and dyall+ts+tp was taken as the uncertainty.

Another source of uncertainty arises from electron correlation. The uncertainty associated with the number of correlated electrons was calculated by comparing the results obtained with the highest and lowest numbers of correlated electrons (47 and 17 electrons respectively) in the calculations. The difference between this results was taken as the uncertainty. Uncertainties coming from the size of the virtual space were computed by taking the difference between calculations at an energy cut-off of 1000 a.u. and 200 a.u.. At last the uncertainty coming from higher triple excitations was obtained by taking double the difference between CCSD+T and CCSD-T. All these uncertainties were squared, summed up and then the square root of this number is taken in order to obtain the total uncertainty for each nuclei. In Table 7 the corresponding uncertainties are shown.

Table 7: Summary of the primary sources of theoretical uncertainty in W_{PV}. All values are expressed as percentages.

Error Source (%)	**F**	**Sr**
Basis Size	1.00	2.13
Diffuse Functions	0.004	0.004
Tight Functions	3.04	-
Higher Excitation	8.42	0.74
Electron Correlation	7.61	7.95
Virtual Space	0.41	0.31
Total (%)	11.80	8.27

The total uncertainty in the final value for fluorine (F) is slightly higher than for the metal atom strontium (Sr). This discrepancy can be primarily attributed to the differing impacts of triple excitations on each atom.As shown in Table 7, the uncertainty arising from higher excitations is more than ten times greater for F than for Sr. Additionally, F has an extra source of uncertainty due to tight functions. It's also important to note that there are other potential sources of uncertainty that could affect the final value for Sr and have not been accounted for. The most significant of these is the treatment of relativistic effects, which can be enhanced in molecules with higher atomic numbers. In order to account for relativistic effects, calculations should be carried out with the addition of the Gaunt term to the Hamiltonian.

This unequal treatment of uncertainties between the two atoms explains the difference in the total uncertainty. Moreover, when examining the remaining sources of uncertainty, we find that both F and Sr are similarly impacted by most computational parameters. However, there is a notable exception concerning the basis set size error: the uncertainty in Sr is double that of F.

In summary, these combined factors account for the total uncertainty in W_{PV} values, highlighting the intricate nature and precision required in such computational analyses. Understanding and addressing these varying sources

of uncertainty is crucial for achieving accurate and reliable results.

The final value for the enhancement factor W_{PV} of F in SrF is ($W_{PV} = 0.240 \pm 0.028$) Hz and for the metal atom Sr is ($W_{PV} = 63.1 \pm 5.2$) Hz. These two final values were calculated using CCSD(T) and with all the electrons in the molecule correlated. Calculations for Sr were done with dyall.v4z basis sets and a virtual space cut-off of 500 a.u.. On the other hand, for F the calculations were done with dyall.v4z + ts + tp basis sets and a vitual space cut-off of 200 a.u..

5.3 Other Molecular Systems

The enhancement factor W_{PV} of the fluorine atom F was calculated for various molecular diatomic systems, and the results are presented in Table 6. Two isoelectronic pairs were tested. In the first pair (SrF and YF+), the results showed that the W_{PV} value in the positive ion YF+ is roughly half that of SrF. Conversely, for the lighter pair (CF and NF+), the W_{PV} value was higher in the positive ion NF+.

This discrepancy can be explained by considering that the enhancement factor W_{PV} is determined by the overlap of the valence electron with the corresponding nucleus, in this case, F. In the first scenario (YF+ and SrF), the primary difference between SrF and YF+ is the addition of an extra proton to the Sr nucleus. This extra proton transforms the Sr nucleus into a Y nucleus and imparts an overall positive charge to the molecule. The increment of positive charge in the heavy nucleus enhances the attraction of the valence electron, resulting in greater localization around the heavy atom and less around the lighter atom F. This could then explain the decrease in W_{PV} for the F atom in YF+ as the valence electron is more localized around the Y atom and hence it interact less with the F nucleus.

For the second case (CF and NF+), the opposite occurs, with the positive ion exhibiting a higher W_{PV} for F. This can be explained by considering that, in a positive ion, the electrons have lower energies, making them more energetically stable and causing them to be localized closer to the nuclear regions. In the case of NF+, the molecule has an overall positive charge, with the highest concentration of positive charge present in the F nucleus due to its higher atomic number compared to N. Since electrons are closer to the nuclear region in positive ions, and in NF+ the concentration of positive charge is in the F atom, the valence electron of NF+ should be more localized around the F atom compared to CF. This could then explain the increase in W_{PV} of F in NF+.

In order to test this, a Mulliken population analysis was also performed when running the calculations. Mulliken population analysis is a method used in computational chemistry to estimate the distribution of electron density among atoms in a molecule. It partitions the total electronic charge density into atomic contributions, providing insight into the charge distribution and bonding characteristics within the molecule. This tool was utilized on the molecules discussed in this section.

When comparing YF+ and SrF, the initial observation was that the primary atomic contribution to the valence electron in both molecules originated from the highest occupied s orbital in the heavy atom, with this contribution being similar for both molecules. However, the p orbital contribution from the heavy atom was three times larger for YF+ than for SrF. Furthermore, YF+ also had a higher contribution from the d orbitals of the heavy element than SrF. The Mulliken analysis results show that the atomic orbital contributions in the heavy atom to the valence electron are greater in YF+ than in SrF. In simpler terms, the valence electron is more localized around the F atom in SrF compared to YF+. Hence explaining the differnce in W_{PV} values.

For CF and NF+, the Mulliken analysis revealed that the primary atomic contributions to the valence electron came from the p orbitals of C and N, rather than F. Although the contributions were similar for both N and C, in NF+ the contribution from N is slightly lower than the one from C in CF. Additionally, the contributions from the p orbitals in the F atom are approximately three times higher in NF+ than in CF. This analysis indicates that the valence electron is more localized around F in NF+, explaining the increased W_{PV} values for the positive ion.

In XeF, the enhancement factor of fluorine increased by several orders of magnitude compared to the other molecular systems, as shown in Table 6. This behavior in the F atom was unexpected. While the W_{PV} value of the heavy atom in XeF should be higher than in SrF due to the higher atomic number of Xe, the W_{PV} value of F was not anticipated to change significantly. Upon further analysis, the Mulliken analysis of XeF revealed that the dominant

atomic contribution to the valence electron came from one of the p orbitals of the fluorine atom. This finding could explain the unexpected increase observed in the enhancement factor W_{PV} of F in XeF.

6 Conclusion

This study investigated the enhancement factor W_{PV} of the fluorine atom in various diatomic molecular systems using different computational methods. For SrF, the enhancement factor W_{PV} was calculated for both nuclei in the molecule. The final recommended value for the enhancement factor W_{PV} of F in SrF is $W_{PV} = 0.240 \pm 0.028$ Hz, and for the metal atom Sr, it is $W_{PV} = 63.1 \pm 5.2$ Hz. The results indicate that the enhancement factor W_{PV} is significantly higher in Sr than in F, demonstrating that the metal atom is more sensitive to NSD-PV effects.

Various computational parameters were adjusted to evaluate their impact on both nuclei. It was observed that the treatment of electron correlation significantly affected the final value of W_{PV} for both atoms, particularly for the fluorine atom, where the CCSD value was more than twice that of the DHF method. The inclusion of triple excitations also altered the final values for both atoms, with pronounced effects on the fluorine atom, highlighting it as the main source of uncertainty, as shown in Table 7. This underscores the importance of carefully selecting computational methods, especially when performing calculations on lighter systems.

Regarding the variation in the size of the active space used in the calculations, results showed that the overall effects on W_{PV} were similar for both Sr and F. However, the fluorine atom exhibited more discrete changes in its enhancement factor as the active space size was gradually increased. This was particularly evident when varying the number of correlated electrons, with the major contribution to the total change in W_{PV} of F resulting from the inclusion of the 1s orbital from fluorine only. This highlights the crucial role of core electron correlation in determining the final W_{PV} value of F.

The enhancement factor was also calculated for other diatomic molecules to compare the differences between molecular systems. Within this group, two isoelectronic pairs (CF, NF+, SrF, and YF+) were studied along with XeF. Results showed that the enhancement factor of F is considerably lower in YF+ than in SrF and higher in NF+ than in CF. In the case of XeF, the enhancement factor of fluorine increased by several orders of magnitude compared to the other molecular systems studied.

Overall, this study emphasizes the crucial role of accurate computational methods, particularly in relation to the enhancement factor W_{PV} of the fluorine atom.

7 References

[1] A. S. Cornell, "Some theories beyond the standard model," in *Journal of Physics: Conference Series*, vol. 645, no. 1. IOP Publishing, 2015, p. 012002.

[2] J. Ginges and V. V. Flambaum, "Violations of fundamental symmetries in atoms and tests of unification theories of elementary particles," *Physics Reports*, vol. 397, no. 2, pp. 63–154, 2004.

[3] M. Safronova, D. Budker, D. DeMille, D. F. J. Kimball, A. Derevianko, and C. W. Clark, "Search for new physics with atoms and molecules," *Reviews of Modern Physics*, vol. 90, no. 2, p. 025008, 2018.

[4] Y. Hao, M. Iliaš, E. Eliav, P. Schwerdtfeger, V. V. Flambaum, and A. Borschevsky, "Nuclear anapole moment interaction in baf from relativistic coupled-cluster theory," *Physical Review A*, vol. 98, no. 3, p. 032510, 2018.

[5] I. B. Zel'Dovich, "Electromagnetic interaction with parity violation," *Sov. Phys. JETP*, vol. 6, no. 6, pp. 1184–1186, 1958.

[6] I. Khriplovich, "Fundamental symmetries and atomic physics," *Physica Scripta*, vol. 2004, no. T112, p. 52, 2004.

[7] W. Haxton, C.-P. Liu, and M. J. Ramsey-Musolf, "Nuclear anapole moments," *Physical Review C*, vol. 65, no. 4, p. 045502, 2002.

[8] E. Gomez, S. Aubin, G. Sprouse, L. Orozco, and D. DeMille, "Measurement method for the nuclear anapole moment of laser-trapped alkali-metal atoms," *Physical Review A*, vol. 75, no. 3, p. 033418, 2007.

[9] V. Flambaum and D. Murray, "Anapole moment and nucleon weak interactions," *Physical Review C*, vol. 56, no. 3, p. 1641, 1997.

[10] C. Wood, S. Bennett, D. Cho, B. Masterson, J. Roberts, C. Tanner, and C. E. Wieman, "Measurement of parity nonconservation and an anapole moment in cesium," *Science*, vol. 275, no. 5307, pp. 1759–1763, 1997.

[11] V. Flambaum and I. Khriplovich, "On the enhancement of parity nonconserving effects in diatomic molecules," *Physics Letters A*, vol. 110, no. 3, pp. 121–125, 1985.

[12] L. Labzovsky, "Doubling and parity non-conservation effects in spectra of diatomic-molecules," *ZHURNAL EKSPERIMENTALNOI I TEORETICHESKOI FIZIKI*, vol. 75, no. 3, pp. 856–867, 1978.

[13] A. Borschevsky, M. Iliaš, V. Dzuba, V. Flambaum, and P. Schwerdtfeger, "Relativistic study of nuclear-anapole-moment effects in diatomic molecules," *Physical Review A*, vol. 88, no. 2, p. 022125, 2013.

[14] V. Dzuba and V. Flambaum, "Parity violation and electric dipole moments in atoms and molecules," *International Journal of Modern Physics E*, vol. 21, no. 11, p. 1230010, 2012.

[15] Y. Hao, P. Navrátil, E. B. Norrgard, M. Iliaš, E. Eliav, R. G. Timmermans, V. V. Flambaum, and A. Borschevsky, "Nuclear spin-dependent parity-violating effects in light polyatomic molecules," *Physical Review A*, vol. 102, no. 5, p. 052828, 2020.

[16] E. B. Norrgard, D. S. Barker, S. Eckel, J. A. Fedchak, N. N. Klimov, and J. Scherschligt, "Nuclear-spin dependent parity violation in optically trapped polyatomic molecules," *Communications Physics*, vol. 2, no. 1, p. 77, 2019.

[17] A. Borschevsky, M. Iliaš, V. Dzuba, K. Beloy, V. Flambaum, and P. Schwerdtfeger, "P-odd interaction constant w a from relativistic ab initio calculations of diatomic molecules," *Physical Review A*, vol. 85, no. 5, p. 052509, 2012.

[18] D. DeMille, S. B. Cahn, D. Murphree, D. A. Rahmlow, and M. G. Kozlov, "Using molecules to measure nuclear spin-dependent parity violation," *Physical review letters*, vol. 100, no. 2, p. 023003, 2008.

[19] T. Isaev and R. Berger, "Electron correlation and nuclear charge dependence of parity-violating properties in open-shell diatomic molecules," *Physical Review A—Atomic, Molecular, and Optical Physics*, vol. 86, no. 6, p. 062515, 2012.

[20] M. Kozlov, A. Titov, N. Mosyagin, and P. Souchko, "Enhancement of the electric dipole moment of the electron in the baf molecule," *Physical Review A*, vol. 56, no. 5, p. R3326, 1997.

[21] N. Mosyagin, M. Kozlov, and A. Titov, "Electric dipole moment of the electron in the ybf molecule," *Journal of Physics B: Atomic, Molecular and Optical Physics*, vol. 31, no. 19, p. L763, 1998.

[22] M. G. Kozlov and L. N. Labzowsky, "Parity violation effects in diatomics," *Journal of Physics B: Atomic, Molecular and Optical Physics*, vol. 28, no. 10, p. 1933, 1995.

[23] T. Isaev, S. Hoekstra, and R. Berger, "Laser-cooled raf as a promising candidate to measure molecular parity violation," *Physical Review A—Atomic, Molecular, and Optical Physics*, vol. 82, no. 5, p. 052521, 2010.

[24] Y. Y. Dmitriev, Y. G. Khait, M. Kozlov, L. Labzovsky, A. Mitrushenkov, A. Shtoff, and A. Titov, "Calculation of the spin-rotational hamiltonian including p-and p, t-odd weak interaction terms for hgf and pbf molecules," *Physics Letters A*, vol. 167, no. 3, pp. 280–286, 1992.

[25] M. Kozlov, V. Fomichev, Y. Y. Dmitriev, L. Labzovsky, and A. Titov, "Calculation of the p-and t-odd spin-rotational hamiltonian of the pbf molecule," *Journal of Physics B: Atomic and Molecular Physics*, vol. 20, no. 19, p. 4939, 1987.

[26] W. Marciano and A. Sanda, "Parity violation in atoms induced by radiative corrections," *Physical Review D*, vol. 17, no. 11, p. 3055, 1978.

[27] C. Patrignani, "Review of particle physics," *Chinese Physics C, High Energy Physics and Nuclear Physics*, vol. 40, no. FERMILAB-PUB-16-568, 2016.

[28] P. J. Mohr and B. N. Taylor, "Codata recommended values of the fundamental physical constants: 1998," *Reviews of modern physics*, vol. 72, no. 2, p. 351, 2000.

[29] N. Stone, "Table of nuclear magnetic dipole and electric quadrupole moments," *Atomic Data and Nuclear Data Tables*, vol. 90, no. 1, pp. 75–176, 2005.

[30] P. Fadeev and V. V. Flambaum, "Time-reversal invariance violation in neutron-nucleus scattering," *Physical Review C*, vol. 100, no. 1, p. 015504, 2019.

[31] A. Geddes, L. Skripnikov, A. Borschevsky, J. Berengut, V. Flambaum, and T. Rakitzis, "Enhanced nuclear-spin-dependent parity-violation effects using the hgh 199 molecule," *Physical Review A*, vol. 98, no. 2, p. 022508, 2018.

[32] A. Kudashov, A. Petrov, L. Skripnikov, N. Mosyagin, T. Isaev, R. Berger, and A. Titov, "Ab initio study of radium monofluoride (raf) as a candidate to search for parity-and time-and-parity–violation effects," *Physical Review A*, vol. 90, no. 5, p. 052513, 2014.

[33] L. Visscher and K. G. Dyall, "Dirac–fock atomic electronic structure calculations using different nuclear charge distributions," *Atomic Data and Nuclear Data Tables*, vol. 67, no. 2, pp. 207–224, 1997.

[34] J. T. Oden, *An introduction to mathematical modeling: a course in mechanics*. John Wiley & Sons, 2011.

[35] P. Atkins, P. W. Atkins, and J. de Paula, *Atkins' physical chemistry*. Oxford university press, 2014.

[36] W. Liu, "Ideas of relativistic quantum chemistry," *Molecular Physics*, vol. 108, no. 13, pp. 1679–1706, 2010.

[37] T. Saue, "Relativistic hamiltonians for chemistry: A primer," *ChemPhysChem*, vol. 12, no. 17, pp. 3077–3094, 2011.

[38] D. Tong, *Quantum Field Theory*. University of Cambridge Part III Mathematical Tripos, 2006, https://www.damtp.cam.ac.uk/user/tong/qft/qft.pdf.

[39] DIRAC, a relativistic ab initio electronic structure program, Release DIRAC19 (2019), written by A. S. P. Gomes, T. Saue, L. Visscher, H. J. Aa. Jensen, and R. Bast, with contributions from I. A. Aucar,

V. Bakken, K. G. Dyall, S. Dubillard, U. Ekström, E. Eliav, T. Enevoldsen, E. Faßhauer, T. Fleig, O. Fossgaard, L. Halbert, E. D. Hedegård, B. Heimlich–Paris, T. Helgaker, J. Henriksson, M. Iliaš, Ch. R. Jacob, S. Knecht, S. Komorovský, O. Kullie, J. K. Lærdahl, C. V. Larsen, Y. S. Lee, H. S. Nataraj, M. K. Nayak, P. Norman, G. Olejniczak, J. Olsen, J. M. H. Olsen, Y. C. Park, J. K. Pedersen, M. Pernpointner, R. di Remigio, K. Ruud, P. Sałek, B. Schimmelpfennig, B. Senjean, A. Shee, J. Sikkema, A. J. Thorvaldsen, J. Thyssen, J. van Stralen, M. L. Vidal, S. Villaume, O. Visser, T. Winther, and S. Yamamoto (available at http://dx.doi.org/10.5281/zenodo.3572669, see also http://www.diracprogram.org).

[40] F. Jensen, *Introduction to computational chemistry*. John wiley & sons, 2017.

[41] C. D. Sherrill, "Basis sets in quantum chemistry," *School of Chemistry and Biochemistry, Georgia Institute of Technology*, 2017.

[42] M. A. Mahmood, B. H. Adil, and K. H. Al Bayati, "33application of gaussian wave functions for 1s states in helium and helium like atoms," *Al-Nahrain Journal of Science*, vol. 16, no. 3, pp. 98–103, 2013.

[43] T. Saue, R. Bast, A. S. P. Gomes, H. J. A. Jensen, L. Visscher, I. A. Aucar, R. Di Remigio, K. G. Dyall, E. Eliav, E. Fasshauer *et al.*, "The dirac code for relativistic molecular calculations," *The Journal of chemical physics*, vol. 152, no. 20, p. 204104, 2020.

[44] J. Styszyński, "Atoms and molecules in relativistic quantum mechanics," in *Journal of Physics: Conference Series*, vol. 104, no. 1. IOP Publishing, 2008, p. 012025.

[45] C. D. Sherrill, "An introduction to hartree-fock molecular orbital theory," *School of Chemistry and Biochemistry Georgia Institute of Technology*, 2000.

[46] V. Magnasco, *Methods of molecular quantum mechanics: An introduction to electronic molecular structure*. John Wiley & Sons, 2009.

[47] A. A. Hasanein and M. W. Evans, *Computational methods in quantum chemistry*. World Scientific, 1996, vol. 5.

[48] J. F. Stanton, "Why ccsd (t) works: a different perspective," *Chemical Physics Letters*, vol. 281, no. 1-3, pp. 130–134, 1997.

[49] L. Visscher, T. J. Lee, and K. G. Dyall, "Formulation and implementation of a relativistic unrestricted coupled-cluster method including noniterative connected triples," *The Journal of chemical physics*, vol. 105, no. 19, pp. 8769–8776, 1996.

[50] I. N. Levine, D. H. Busch, and H. Shull, *Quantum chemistry*. Pearson Prentice Hall Upper Saddle River, NJ, 2009, vol. 6.

[51] E. G. Lewars, "Computational chemistry," *Introduction to the theory and applications of molecular and quantum mechanics*, vol. 318, 2011.

[52] C. J. Cramer, F. Bickelhaupt *et al.*, "Essentials of computational chemistry," *ANGEWANDTE CHEMIE-INTERNATIONAL EDITION IN ENGLISH-*, vol. 42, no. 4, pp. 381–381, 2003.

[53] N. Brassington, H. Edwards, and D. Long, "Pure rotational raman spectrum of xef 2," *Journal of the Chemical Society, Faraday Transactions 2: Molecular and Chemical Physics*, vol. 74, pp. 1208–1213, 1978.

[54] M. V. Ivanov, T.-C. Jagau, G.-Z. Zhu, E. R. Hudson, and A. I. Krylov, "In search of molecular ions for optical cycling: a difficult road," *Physical Chemistry Chemical Physics*, vol. 22, no. 30, pp. 17 075–17 090, 2020.

[55] Wikipedia, "Angstrom," https://es.wikipedia.org/wiki/%C3%81ngstrom, (Accessed 9 June 2023).

[56] R. Barrow and J. Beale, "The internuclear distance in gaseous srf," *Chemical Communications (London)*, no. 12, pp. 606a–606a, 1967.

[57] T. H. Dunning Jr, W. P. White, R. M. Pitzer, and C. W. Mathews, "The electronic states of carbon monofluoride: Low-lying valence states," *Journal of Molecular Spectroscopy*, vol. 75, no. 2, pp. 297–317, 1979.

[58] J. M. Dyke, N. Jonathan, A. E. Lewis, and A. Morris, "Vacuum ultraviolet photoelectron spectroscopy of transient species. part 14.—a study of the ground state of nf+ via the ionization processes nf+(x 2 π) â† nf (x 3 σ–, a 1 δ)," *Journal of the Chemical Society, Faraday Transactions 2: Molecular and Chemical Physics*, vol. 78, no. 8, pp. 1445–1450, 1982.